Clays and Clay Minerals, Vol. 62, No. 5, 425–446, 2014.

EFFECTS OF CHEMICAL STRUCTURE ON THE STABILITY OF SMECTITES IN SHORT-TERM ALTERATION EXPERIMENTS

Lan Nguyen-Thanh[1,2,*], Horst-Jürgen Herbert[3], Jörn Kasbohm[2], Thao Hoang-Minh[4], and Rafael Ferreiro Mählmann[1]

[1] Technical Petrology, Institute of Applied Geosciences, Technische Universität Darmstadt, Schnittspahnstr. 9, 64287 Darmstadt, Germany
[2] Institute of Geography and Geology, Ernst-Moritz-Arndt-University of Greifswald, Friedr.-Ludwig-Jahn-Str. 16, 17487 Greifswald, Germany
[3] Gesellschaft für Anlagen- und Reaktorsicherheit mbH, Theodor-Heuss-Str. 4, 38122 Braunschweig, Germany
[4] VNU University of Science, 334 Nguyen Trai road, Thanh Xuan district, Hanoi, Vietnam

Abstract—Because of their isolating capacity, smectite-rich clays have been proposed as buffer and backfill materials in high-level radioactive waste repositories. These repositories have to guarantee long-term safety for ~1 million years. Thermodynamics and kinetics of possible alteration processes of bentonite determine its long-term performance as a barrier material. Smectites in 25 different clays and bentonites were investigated in order to identify possible differences in their rates of alteration. These samples were saturated for 30 days in 1 M NaCl solution and deionized water, and then overhead rotated at speeds of 20 rpm and 60 rpm. Depending on the octahedral and interlayer composition, each of the smectites studied had specific rate of alteration, a so-called specific dissolution potential of smectite. The bentonites were classed as 'slow-reacting bentonite', 'moderate-reacting bentonite', or 'fast-reacting bentonite' corresponding to a relatively low (ΔP – specific dissolution potential – $<-5\%$), moderate ($-5\% < \Delta P < -20\%$), or high specific dissolution potential ($\Delta P > -20\%$), respectively. The larger the amount of octahedral Fe and Mg compared to octahedral Al, the greater the specific dissolution potential. The present study found that the interlayer composition has a discernible impact on the rate of alteration. In experiments with rotation speeds of 60 rpm and a 1 M NaCl solution, Na^+ was found to be the stabilizing cation in the interlayers of all the smectites. The Na-stabilizing mechanism was identified in only some of the smectites (type A) in experiments with 20 rpm (1 M NaCl solution). A second stabilization mechanism (by interlayer cations; Ca and Mg) was identified for other smectites (type B). Each bentonite has a specific rate of alteration. 'Slow-reacting bentonite' and clay with smectite-illite interstratifications are recommended as potential clay barriers in HLW repositories. The experimental and analytical procedures described here could be applied to potential barrier materials to identify 'slow-reacting bentonite'.

Key Words—Bentonites, Clay Stability, Interlayer Composition, Octahedral Sheet Composition, Overhead Rotating, Short-term Alteration, Smectite, Specific Dissolution Potential.

INTRODUCTION

Bentonites are considered suitable buffer- and backfill-materials in the multibarrier concept for high-level radioactive waste (HLW) repositories. In Germany, the current storage concept requires the ability to predict the behavior of bentonites in geotechnical barriers over a period of 1 million years in salt host rock (BGR, 2007). The desired characteristics of bentonites include large swelling capacities to promote self-sealing and very low hydraulic conductivities (Pusch, 1992; Pusch and Yong, 2006). The alteration of smectites, however, depends on several factors including fluid composition, temperature, pH, and initial smectite composition, all of which influence the physicochemical properties of smectites and their stability. The intrusion or upwelling of saline groundwater or salt deposition in the buffer material during the re-saturation phase, or salt extraction from the cement used in construction, may make available large concentrations of Na^+, Ca^{2+}, or even K^+ and Mg^{2+} cations (Stober and Bucher, 2002; Pearson *et al.*, 2003; SKI, 2005). Where granite is the host rock, the water-flow rate along the interface between it and the barrier may cause hydroxylation exchange, transport of dissolved cations and grain-boundary diffusion (Pusch, 1999b).

Several studies have investigated the stability of bentonites in contact with different solutions under variable environmental conditions. For example, Adamcova *et al.* (2008), Suzuki *et al.* (2008), and Kaufhold and Dohrmann (2009, 2011) focused their studies on changes in geotechnical parameters; *e.g.* the swelling pressure or cation exchange capacity (CEC). Others have described a reduction in CEC and swelling pressure or increased hydraulic conductivity and porosity in experiments with smectites at low temperatures (Bildstein *et al*., 2006; Carlson *et al*., 2007; Perronnet *et al*., 2008; Ishidera *et al*., 2008; Marty *et al*., 2010). The

* E-mail address of corresponding author:
nguyen@geo.tu-darmstadt.de
DOI: 10.1346/CCMN.2014.0620506

decrease in swelling pressure with increasing salinity has been proposed to result mainly from ionic-strength effects of the osmotic pressure of water between clay particles, together with the effects of varying ionic compositions on the hydration potential in interlamellar spaces between clay particles (Pusch, 2002; SKI, 2005; Herbert *et al*., 2008). Kaufhold and Dohrmann (2009, 2010, 2011) discussed the decreasing CEC as being caused by the collapse of particles, particularly of highly charged smectites. A collapse of particles caused by large ionic strength generally reduced the swelling pressure (Dixon *et al.*, 1996; Karnland *et al.*, 2006; Castellanos *et al.*, 2008; Herbert *et al.*, 2008). The stability of two-water-layer coordination in the interlayer may be altered as a result of changes in asymmetry, and the shift of the d_{001} value could also be interpreted as being due to hydration heterogeneity as suggested by Bauer *et al.* (2001), Ferrage *et al.* (2005), and Kaufhold and Dohrmann (2009). Although changes in the geotechnical properties of the clay minerals were accepted, these results cannot be explained without the occurrence of some form of mineralogical alteration of smectite phases.

Mineralogical-chemical smectite transformation, *e.g.* transformation of montmorillonite to a non-expandable or less-expandable clay mineral, is expected to be caused by a thermodynamically driven process which would reduce the value of bentonite as a backfill or buffer material in HLW repositories. The transformation of smectite to illite or vermiculite has been a main focus of research in recent years and was discussed in detail by Pusch and Kasbohm (2002), Honty *et al.* (2004), Meunier and Velde (2004), Charpentier *et al.* (2006), Kaufhold *et al.* (2010), and Mosser-Ruck *et al.*(2010). On the other hand, the conversion of montmorillonite to beidellite and beidellite to illite was noted by SKI (2005) and Karnland *et al.* (2007). Furthermore, conversion of montmorillonite to kaolinite or pyrophyllite in a chemically closed system was discussed by Herbert *et al.* (2004) and Kasbohm *et al.* (2004). Changing the microstructure of smectite by Si precipitation was described by Pusch (1999a). Alteration of the stacking order of smectite particles accompanied by changes in the chemical composition of octahedral sheets in low-temperature experiments was also shown by Herbert *et al*. (2004, 2008). In summary, chemical composition, ordering, and pseudomorphism are all considered to contribute to the alteration of the mineralogical structure of smectites.

The present study aimed to clarify the mineralogical-chemical alteration processes taking place in smectites exposed to 1 M NaCl solution or to deionized water. These two agents were selected to identify the impact of different ionic strengths and to simulate the possible solutions in repositories in granite or clay as host rock (low ionic strength) and in salt rock (high ionic strength). A series of 25 bentonites and clays were included in the study. The initial hypothesis was that the alteration process can be accelerated by large quantities of Fe and Mg in mineral octahedral sheets (Čičel and Novak, 1977) and that some smectites can be protected by large concentrations of Ca^{2+} in the interlayers (Kaufhold and Dohrmann, 2008). Furthermore, increased ionic strength should promote faster alteration. Representative materials of Na-smectite, Ca-smectite and Fe-rich smectite were therefore used in this research. The present study aimed to identify the rate of alteration or so-called 'specific dissolution potential' of smectites which varied with the interlayer and octahedral composition. Based on their specific dissolution potential, the bentonites of high, medium, and low stability are termed 'slow-reacting bentonite' (SR-B), 'moderate-reacting bentonite' (MR-B), and 'fast-reacting bentonite' (FR-B), respectively. Transmission electron microscopy equipped with energy-dispersive X-ray (TEM-EDX), X-ray diffraction (XRD), Fourier transform infrared spectroscopy (FTIR), and X-ray fluorescence (XRF) analyses were used to identify possible mineralogical alteration processes.

MATERIALS, EXPERIMENTS, AND ANALYTICAL METHODS

Materials and experiments

The following materials were used: 12 bentonites from the BGR (Bundesanstalt für Geowissenschaften und Rohstoffe, Hannover, Germany) collection (04F, 09F, 11F, 12F, 13F, 16F, 22F, 23F, 28F, 31F, 37F, 38F); nine bentonites of the API (American Petroleum Institute Clay Mineral Standards) series [Polkville, Mississippi (API #20), Amory, Mississippi (API #22a), Chambers, Arizona (API #23), Otay, California (API #24), Belle Fourche, South Dakota (API #27), Bayard, New Mexico (API #30), Pioche, Nevada (API #32), Cameron, Arizona (API #31), and Garfield (nontronite), Washington (API #33a)], MX80 (a commercial product, obtained from Süd-Chemie AG, Moosburg, Germany in 2005), and illite-smectite interstratified structures (I-S-ml) bearing clays such as Friedland clay (taken from core TB97/1 of the ore body from 'Burgfeld Scholle' quarry, Germany), GeoHellas clay (from western Macedonia, Greece, sample DA1206-02), and Vietnam clay (from Nui Nua, Thanh Hoa province, north central Vietnam).

These 25 different samples of bentonites and clays were ground to <40 μm and dispersed at a liquid:solid ratio of 4:1 in 1 M NaCl solution or at 10:1 in deionized water. The resulting soft gels were agitated mechanically by means of a consistent uniform rotating motion at constant speed (overhead rotating) at room temperature for 30 days at a rate of 20 revolutions per minute (rpm) or 60 rpm. This experiment assumes that the greater the speed of overhead rotating, the greater will be the removal of dissolved elements from the mineral phases.

https://doi.org/10.1346/CCMN.2014.0620506 Published online by Cambridge University Press

The amount of dissolved ions removed at 60 rpm is greater than that at 20 rpm.

The reaction products after treatment in 1 M NaCl solution were dialyzed in a 2 mL capsule (semipermeable membrane) of the microdialysis QuixStep®-system (IKA® Big Squid magnetic stirrers instrument of IKA-Werke GmbH & Co. KG, Germany) for 1 h to remove NaCl. A magnetic stirrer was used to rotate the capsule in the dialysis beaker; this process diffused Na^+ across the membrane layer and removed NaCl from the reaction products. The uncontaminated NaCl reaction products are indicated by the lack of flocculation of clay particles. The initial materials and reaction products were compared and characterized mainly through TEM-EDX analyses.

Analytical methods

The chemical composition of samples was analyzed using a wavelength-dispersive X-ray Philips PW 2404 spectrometer equipped with a 4 kW Rh X-ray source (10 mA, 20 kV) of X-ray fluorescence (XRF). The samples were milled, prepared by mixing 8 g of the sample with 2 g of lithium tetraborate in 40 mm pellets which were pressed under a pressure of 160 bars. The measurements were carried out under vacuum and analyzed with a non-wetting agent and/or oxidizer to remove free water. Loss on ignition (LOI) was determined at 1100ºC as an approximate measure of volatile H_2O.

For XRD analysis, randomly oriented powder mounts of bulk samples and oriented mounts, including air-dried, ethylene-glycolated, and heated specimens (550ºC for 4 h) of the <2 μm fraction were analyzed using a Siemens D5000 X-ray diffractometer (Cu tube, $K\alpha_{1,2}$ radiation, 40 kV, 30 mA) (Brucker AXS GmbH, Germany). The oriented sample mounts were preprared by mixing 45 mg of the clay (<2 μm) with 1.5 mL of deionized water and pipetting the mixed solution onto glass slides and drying under atmospheric conditions overnight at room temperature. Fe-rich samples were measured using a Freiberg Präzitronic diffractometer HZG 4A-2 (VEB Freiberger Praezisionsmechanik, Germany) equipped with a Seifert C3000 control unit (Co tube, $K\alpha_{1,2}$ radiation, 30 kV, 30 mA). The XRD data were processed using BGMN-Rietveld software (Bergmann *et al.*, 1998; Ufer *et al.*, 2004, 2008; Kleeberg *et al.*, 2010) and constrained by X-ray fluorescence (XRF) results.

The FTIR spectra of bulk samples were recorded over the 400−4000 cm^{-1} range using a Nicolet 6700 FTIR Spectrometer (Thermo Scientific brand of Thermo Fisher Scientific, Inc., Germany) (64 scans, 4 cm^{-1} resolution). The FTIR spectra were deconvolved using *Origin Pro Peak Fitting* (version 8.5) (© OriginLab Corporation). Interpretation of individual bands followed Farmer and Russell (1964), Goodman *et al.* (1976), Craciun (1984), Madejová *et al.* (1994), and Madejová and Komadel (2001).

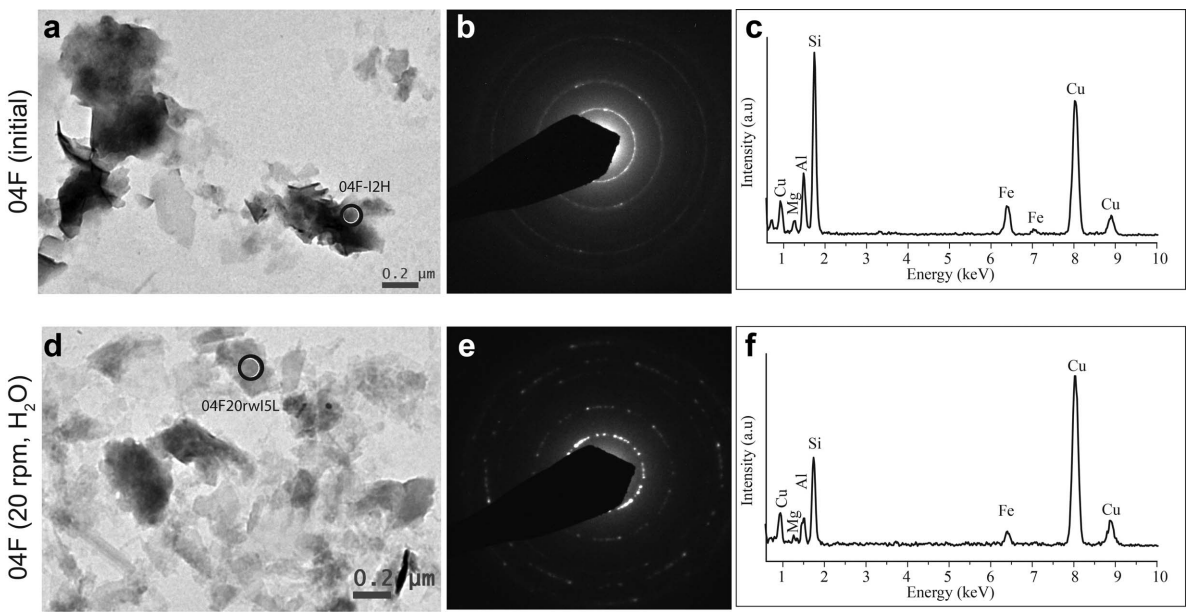

Figure 1. TEM measurements of particles in sample 04F: (a,d) morphology; (b,e) electron diffraction; and (c,f) element distribution. (a−c) Original material; and (d−f) after treatment for 30 days in deionized water at 20 rpm of overhead rotation. Note: circle in parts a, d = data point for electron diffraction and EDX spectra; (a,d) particle shaped mainly as xenomorphous plates, with partially rolled edges; (b) turbostratic order of particles; (c) EDX spectra (montmorillonite, see Table 1, example 1); (e) multiple particles in the measured aggregate developing 1*M* polytype order; (f) EDX spectra (montmorillonite, see Table 1, example 2).

https://doi.org/10.1346/CCMN.2014.0620506 Published online by Cambridge University Press

Table 1. General schema for the calculation of mineral formula based on TEM-EDX analyses according to Köster (1977) and Kasbohm *et al*. (2002).
Example 1: TEM-EDX measurement point 04F-I2H, Sample 04F initial (Figure 1a) = montmorillonite.

TEM-EDX analysis		Conversion (according to Köster, 1977)			Number of cations	Model of mineral formula			—— Controlling ——	
Element	Atom.%	Charge	Equiv./ charge	Cat. val./ formula unit	No. Cat./ formula unit	Sheet	Ele-ment	Index	Cations per sheet	Sum of charges
(1)	(2)	(3)	(4)	(5)	(6)	(7)	(8)	(9)	(10)	(11)
Na	0.00	+1					Na^{+}	0.00		
K	0.10	+1	0.10	0.015	0.015	Interlayer space	K^{+}	0.02	$n^{XII} = 0.14$	0.25
Mg	1.61	+2	3.22	0.499	0.249		Mg^{2+}	0.06		
Ca	0.40	+2	0.80	0.124	0.062		Ca^{2+}	0.06		
Fe	4.00	+3	12.00	1.859	0.620		Fe^{3+}	0.62		
Al	8.04	+3	24.12	3.736	1.245	Octahedral sheet	Al^{3+}	1.19	$n^{VI} = 2.00$	−0.19 [6−Σcharges]
Si	25.45	+4	101.80	15.767	3.942		Mg^{2+}	0.19		
O	60.04					Tetrahedral sheet	Al^{3+}	0.06	$n^{IV} = 4.00$	−0.06 [16−Σcharges]
P	0.05						Si^{4+}	3.94		
S	0.11						O^{2-}	10		
Cl	0.27						OH^{-}	2		
Sum	100.07									
	Sum of equivalents		142.04							Total sum = 0.00
	Postulated total charge		22							

Example 2: TEM-EDX measurement Point 04F 20rwI5L, Sample 04F, 20 rpm, H_2O (Figure 1b) = montmorillonite.

TEM-EDX analysis Element		Conversion (according to Köster, 1977)			Number of cations	Model of mineral formula			—— Controlling ——	
	Atom.%	Charge	Equiv./ charge	Cat. val./ formula unit	No. Cat./ formula unit	Sheet	Ele- ment	Index	Cations per sheet	Sum of charges
(1)	(2)	(3)	(4)	(5)	(6)	(7)	(8)	(9)	(10)	(11)
Na	0.00	+1					Na^{+}	0.00		
K	0.00	+1					K^{+}	0.00		
Mg	1.72	+2	3.44	0.664	0.332	Interlayer space	Mg^{2+}	0.11	$n^{XII} = 0.13$	0.25
Ca	0.10	+2	0.20	0.039	0.019		Ca^{2+}	0.02		
Fe	1.60	+3	4.80	0.927	0.309		Fe^{3+}	0.31		
Al	7.71	+3	23.13	4.466	1.489	Octahedral sheet	Al^{3+}	1.44	$n^{VI} = 2.00$	−0.20
Si	20.45	+4	81.80	15.796	3.949		Mg^{2+}	0.23		[Σcharges−6]
O	66.11						Ti^{4+}	0.03		
Ti	0.14	+4	0.56	0.108	0.027	Tetrahedral sheet	Al^{3+}	0.05	n^{IV} =	−0.05
							Si^{4+}	3.95	4.00−0.06	[Σcharges−16]
							O^{2-}	10		
Sum	100.07						OH^{-}	2		
		Sum of equivalents	113.93							Total sum = 0.00
		Postulated total charge	22							

Notes: Fe as Fe^{3+} and total charge of 22 are postulated parameters in the case of assumed dioctahedral 2:1 sheet silicate); Equiv./charge = distribution of elements as equivalents with charge [column 4], calculated by multiplying the distribution of elements [column 1] analyzed by TEM-EDX [column 2] and charge of corresponding element [column 3]; Cat. Val./formula unit = total cation value per unit cell factor [column 5], calculated by Equiv./charge [column 4] multiplied by the total charge of the unit cell and then divided by the sum of equivalents; No. Cat./formula unit = number of cations per unit cell factor [column 6], calculated by dividing Cat. Val./ formula unit [column 5] by charge [column 3]; ΣCat. and ΣCharge/formula unit = total cations and total charge per unit cell factor; XII − interlayer charge; n^{XII} = number of interlayer cations; VI = octahedral charge; n^{VI} = number of cations per octahedral sheet; IV = tetrahedral charge; n^{IV} = number of cations per tetrahedral sheet.

Selected individual clay particles were characterized by morphology (size, shape) and crystal habits of smectite particles, chemical composition, electron diffraction pattern, and element distribution (Figure 1) using a JEOL JEM-1210 microscope (120 kV, LaB_6 cathode) coupled with an ISIS LINK-OXFORD EDX system. Samples were prepared by suspending clay on carbon-coated Cu-grids and air-drying. Mineral formulae were calculated using semi-quantitative data from ~100 particles per sample based on the system of Köster (1977) and the software toolkit of Kasbohm *et al.* (2002) (Table 1). The smectitic layer ratio (%*S*) was calculated using the TEM data as proposed by Środón *et al.* (1992):

$$\%S = 100.38\ (Al_{IV})^2 - 213\ Al_{IV} + 100.25 \quad (1)$$

The rate/degree of alteration (Δ%*S*), referred to below as the "changed smectitic layer ratio", was calculated by the difference between the smectitic layer ratio of the reaction products after the experiment ($\%S_{experiment}$) and the smectitic layer ratio of the initial materials ($\%S_{origin}$):

$$\Delta\%S = \%S_{experiment} - \%S_{origin} \quad (2)$$

The alteration processes of bentonite were classed empirically either as illitization (Si mitigation) if Δ%*S* <0 (regardless of the amount of K) or smectitization (Si enrichment) if Δ%*S* >0.

*Calculation of specific dissolution potential (Δ*P*) of smectite*

The measured Δ%*S* values were also used to identify the impact of alterations based on the initial interlayer cation and initial octahedral cation composition, flow rate of fluid movement from overhead rotation removing dissolved Si and other cations (Δ*P*o) as well as the specific dissolution potential (Δ*P*) of the smectites. For each of the experiments, the rate of alteration influenced by the initial interlayer cations (ΔP_{XII}) of smectites was estimated using a correlation equation modeled by the measured Δ%*S* and the initial interlayer Na/(Na+Ca+Mg) (the so-called Na-ratio) (Figure 2a) for samples with similar octahedral ratios (Fe+Mg)/(Fe+Mg+Al) (Fe+Mg-ratio). The rate of alteration affected by initial octahedral composition (ΔP_{VI}) of smectites was estimated using a correlation equation modeled by the measured Δ%*S* and the initial octahedral Fe+Mg-ratio for samples with similar Na-ratio (Figure 2b). The specific dissolution potential of smectite (Δ*P*) was finally defined as the sum of the two parameters (ΔP_{XII} and ΔP_{VI}). The changed smectitic layer ratio (Δ%*S*) was also used to evaluate Δ*P* and Δ*P*o. The value of the Δ*P*o coefficient depended on the speed of rotation and the solution conditions of the experiments. This parameter was determined empirically for each experimental design from the observed sudden change of the Δ%*S* values from strong illitization to slight smectitization.

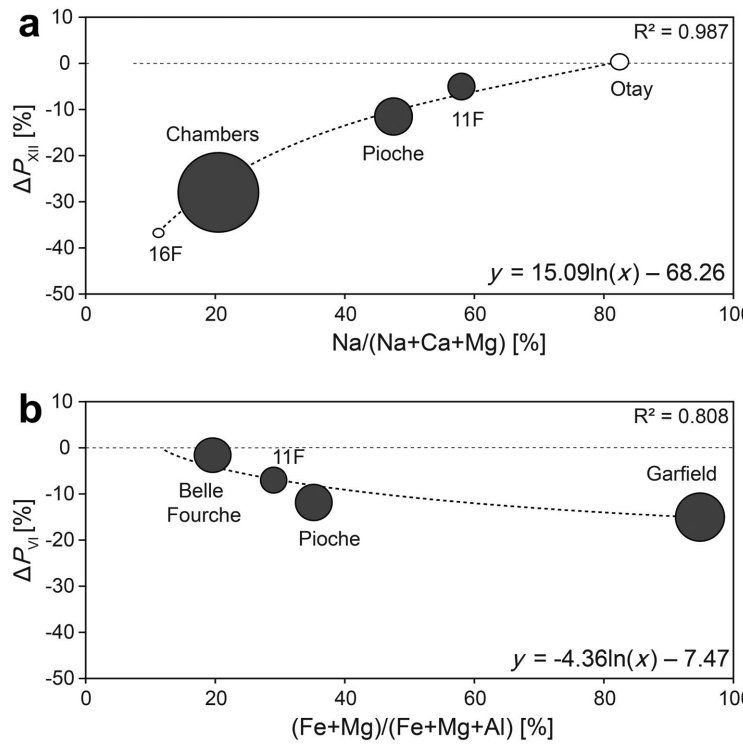

Figure 2. Empirical determination of impact by (a) initial interlayer cations ΔP_{XII} and (b) initial octahedral cations ΔP_{VI} on specific dissolution potential, Δ*P*, for experimental series: 60 rpm + NaCl. Note: $\Delta P = \Delta P_{XII} + \Delta P_{VI}$; the diameter of the circles is related to the measured decrease of smectitic layer ratio, %*S*, between the original and treated smectites.

https://doi.org/10.1346/CCMN.2014.0620506 Published online by Cambridge University Press

RESULTS

Mineralogical characteristics of initial materials

API bentonites. The mineralogical compositions of the API bentonites revealed that montmorillonite is the most abundant phase in eight bentonites but the Garfield sample is dominated by nontronite (Table 2). The FTIR spectra of the API bentonites were obtained at the California Institute of Technology (API Clay Mineral Standards) and processed during the present study. Three major bands, Al-OH-Al (905–916 cm^{-1}), Al-OH-Fe (871–881 cm^{-1}), and Al-OH-Mg (835–849 cm^{-1}) in OH-bending regions were observed in all bentonites. The Garfield sample showed an Fe-OH-Fe band at 816 cm^{-1} for nontronite and 3543 cm^{-1} and 3567 cm^{-1} bands in the OH-stretching region characteristic of montmorillonite. All of the bentonites, except the Bayard bentonite, exhibited two bands at 778 cm^{-1} and 798 cm^{-1}, which were related to the Si–O stretching bands of quartz.

BGR bentonites. Twelve untreated bentonites from the BGR series were investigated. Sample localities were not given (Kaufhold *et al.*, 2008) because most of the samples were provided by bentonite-producing companies. The BGR has already published some parameters, including chemical composition, degree of detachment of colloid particles, pH of aqueous bentonite suspensions, CEC, and exchangeable cations (Kaufhold and Dohrmann, 2008, 2013; Kaufhold *et al.*, 2008) including qualitative and quantitative mineral compositions (Ufer *et al.*, 2008), and carbonate and sulfur concentrations (Kaufhold *et al.*, 2008). Measurements by transmission electron microscopy-energy dispersive X-ray (TEM-EDX) verified that dioctahedral smectites are the dominant phase and confirmed a very high smectitic layer ratio (Table 3; other than sample 13F). The FTIR measurement showed the dominance of montmorillonite not only in the OH-stretching but also in OH-bending regions in all of the BGR bentonite samples studied. Three major bands, Al-OH-Al at 905–913 cm^{-1}, Al-OH-Fe at 872–891 cm^{-1}, and Al-OH-Mg at 834–865 cm^{-1}, were identified in the OH-bending regions. All the FTIR spectra exhibited two bands at 779 cm^{-1} and 799 cm^{-1}, which can be assigned to the Si-O bending vibration of quartz or cristobalite.

Other clays. The GeoHellas clay had an Fe-rich illite-smectite interstratified structure, saponite, palygorskite, chlorite, quartz, dolomite, Mg-bearing calcite, orthoclase, plagioclase, and goethite (Table 2). The FTIR spectrum of this clay was characterized by an OH-stretching band at 3546 cm^{-1}, an OH-bending band at 820 cm^{-1}, as well as a Si-O-Fe band at 491 cm^{-1}, which is indicative of substitution of tetra-

Table 2. Mineral composition of the bentonites and clays studied as determined from XRD data with BGMN-Rietveld refinement.

Samples/ phases (wt.%)	Polkville #20	Amory #22a	Chambers #23	Belle Fourche #27	Bayard #30	Cameron #31	Pioche #32	Garfield #33a	MX80 (2005)	Friedland	Geo-Hellas	Vietnam
Smectite	95	84	89	86	96	79	65	38	77	20	37	87
IS-ml										36		
Nontronite								60				
CSV-ml											5	
Palygorskite											12	
Saponite											3	
Illite		1					6			2		
Muscovite									1			
Chlorite		+					4			1	4	4
Kaolinite						1	5			14		4
Quartz	3	3	3		8	20	3	2	5	20	8	2
Cristobalite									3			
Calcite	2		8				16		+		4	
Dolomite											6	
Gypsum										+		
Hematite						+						
Magnetite							+					+
Microcline		12										
Albite				6	4				13	4	12	
Pyrite										+		
Antigorite												+
Talc												3

Notes: IS-ml: illite-smectite interstratified phase and CSV-ml: chlorite-saponite-trioctahedral vermiculite interstratified phase; smectite includes IS-ml and dioctahedral vermiculite-smectite interstratified phase (diVS-ml), (+) trace phase. The mineral compositions of the BGR samples was published by Ufer *et al.* (2008).

https://doi.org/10.1346/CCMN.2014.0620506 Published online by Cambridge University Press

hedral Fe^{3+} for Si in smectite. The GeoHellas clay was dominated by an Fe-rich illite-smectite interstratified structure rather than by saponite, in agreement with assessments by Christidis *et al.* (2010).

The Vietnam clay consists mainly of an Fe-rich illite-smectite interstratified phase as shown by XRD (Table 2) and TEM-EDX (Table 3) and confirmed by FTIR analysis (Nguyen-Thanh *et al*., 2014).

The Friedland clay was also dominated by an Fe-rich illite-smectite interstratified structure (see Tables 2, 3). The FTIR scans of the Friedland clay showed a strong distinct OH bend at 915 cm^{-1}, which was assigned to the Al-OH-Al band seen in Al-smectite and kaolinite (Farmer, 1974). The Al-OH-Fe^{3+} band at 876 cm^{-1} had low intensity reflecting the significantly higher Fe^{3+} content in the octahedral sheet of the Friedland clay. Bending at 828 cm^{-1} was assigned to Al-OH-Mg. The Al-O vibrations in the illite lattice structure appeared at 753 cm^{-1}. Friedland clay thus contains quartz as determined by FTIR, XRD, and TEM-EDX. Traces of pyrite were detected in XRD patterns at 1.62 Å only (Nguyen-Thanh, 2012).

Analysis by XRD of MX80 bentonite (product tradename from 2005) showed smectite as the major phase (Table 2). This phase was dominated by Al in the octahedral sheet and had less Na in the interlayer (Table 3) than did the MX-80 smectite documented by previous investigations by Madsen (1998), Herbert *et al.* (2004), and Hoang-Minh (2006). The FTIR analysis showed a broad absorption band at 3624 cm^{-1} (Al-OH-Al) in the OH-stretching and at 916 cm^{-1} in the OH-bending regions. This reflects the large Al content in the octahedral sheet structure. The bands at 875 cm^{-1} and 846 cm^{-1} correspond to Al-OH-Fe and Al-OH-Mg, respectively. The sharp band at 779 cm^{-1} indicated the occurrence of quartz. The bands at 796 cm^{-1} and 617 cm^{-1} are typical of cristobalite.

Characterization of reaction products after overhead rotating experiments

In order to determine the stability of smectites in short-term experiments, changes in the composition of the initial materials and the reaction products were investigated by TEM-EDX. This method allowed us to accurately distinguish the chemical structures of very fine (<2 μm) components of the samples.

Highly transport-controlled alteration experiments in contact with 1 M NaCl-solution (60 rpm + NaCl). Eleven bentonites were tested in rapid overhead rotating experiments with 1 M NaCl-solution (60 rpm + NaCl). Any possible alteration should be controlled mainly by transport processes. Comparing the mineral formulae of the initial materials (Table 3) with the reaction products (Table 4) showed that the interlayer charge (XII) usually increased during the experimental run. A larger Na content in the interlayer, furthermore, appeared to protect smectite against Si mitigation (Figure 3). The original Na-ratio in the interlayer ranged from the smallest value in the Chambers and 09F bentonites, through intermediate values in the Pioche, Belle Fourche, and 11F bentonites, to the largest values in the Otay bentonites. This increase in Na-ratio correlated with a decrease in Si mitigation (*i.e.* increase in Δ%*S*) in the reaction products of these smectites. An enhanced Si mitigation was seen in the Garfield bentonite, which has

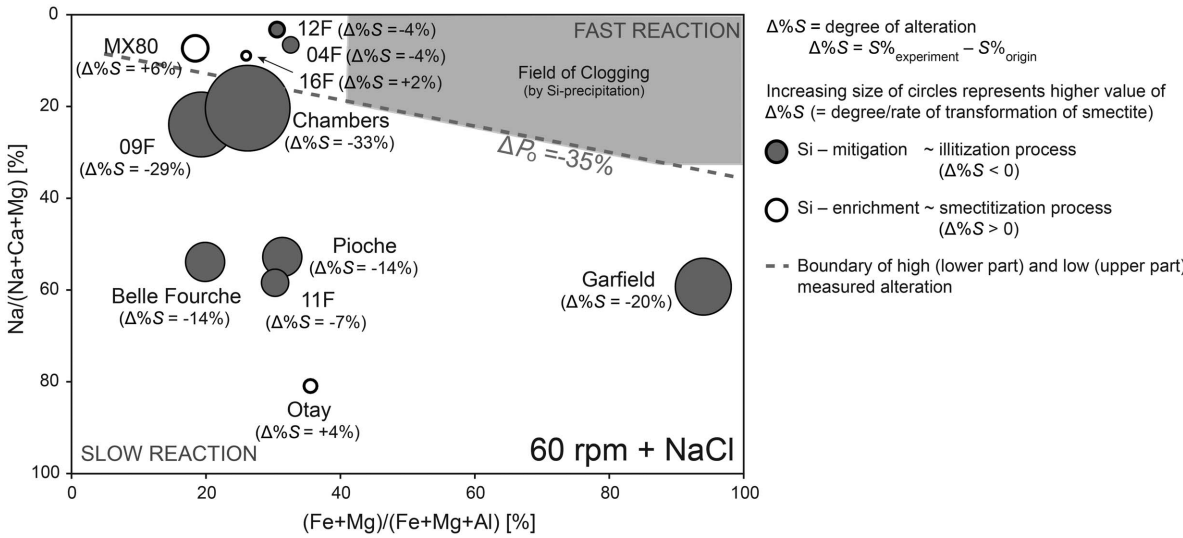

Figure 3. Smectitization and illitization caused by the (60 rpm + NaCl) experiment using a flow rate of shaking $\Delta Po = -35\%$ (maximal alteration by flow rate of shaking). Note that the horizontal and vertical axes represent the original compositions of the smectites. The diameters of the circles are related to the measured loss or increase of smectitic layer ratio, %*S*, between the original and the treated smectite (see note in Figure 2).

https://doi.org/10.1346/CCMN.2014.0620506 Published online by Cambridge University Press

Table 3. Chemical analysis of major elements by TEM-EDX (atom.%) and calculated mineral formula (cations per $[O_{10}(OH)_2]$) for mean of dioctahedral smectites from initial studied materials.

Sample	04F	09F	11F	12F	13F	16F	22F	23F	28F	31F	37F	38F	#20	#22a	#23	#24	#27	#30	#32	#31	#33a	MX	Frd	GH	VN
Chemical analyses of major elements (atom.%) by TEM-EDX																									
Elements																									
O	62.8	66.1	63.0	65.7	65.5	65.9	68.6	68.3	68.2	69.3	65.8	66.9	61.4	63.4	63.9	67.2	63.0	62.9	61.2	62.7	67.9	70.0	51.6	62.0	67.1
Na	0.1	0.3	1.0	0.0	0.0	0.1	0.1	0.0	0.0	0.0	0.0	0.0	0.6	0.5	0.4	1.0	1.8	0.8	1.3	0.8	0.3	0.0	0.2	0.0	0.0
Mg	1.6	1.5	1.5	1.9	1.0	1.5	1.8	1.6	2.1	1.9	1.5	1.3	1.9	1.2	2.4	0.9	1.3	3.2	2.6	1.2	0.2	0.9	1.8	3.5	1.4
Al	8.8	8.6	8.2	7.0	8.8	8.7	8.2	8.6	7.7	6.6	9.3	8.4	9.6	9.0	8.5	7.4	9.3	8.2	9.1	10.7	3.2	7.8	14.5	7.1	4.0
Si	22.8	20.5	22.5	21.3	20.7	21.6	19.8	20.4	20.4	19.4	22.1	20.7	23.6	23.0	22.4	18.6	22.2	23.9	22.7	21.0	18.2	19.1	26.9	22.1	19.6
K	0.3	0.1	0.1	0.1	0.3	0.2	0.1	0.1	0.0	0.3	0.1	0.1	0.1	0.1	0.0	0.3	0.2	0.1	0.3	1.0	0.1	0.1	1.7	0.7	0.2
Ca	0.3	0.6	0.2	1.3	0.5	0.2	0.4	0.2	0.3	0.2	0.1	0.4	0.2	0.1	0.9	0.1	0.2	0.1	0.1	0.1	0.1	0.2	0.1	0.7	0.2
Ti	0.1	0.0	0.1	0.1	0.1	0.0	0.0	0.1	0.1	0.1	0.1	0.1	0.0	0.1	0.1	0.1	0.1	0.1	0.1	0.0	0.0	0.2	0.2	0.1	0.2
Cr	0.0	0.0	0.0	0.0	0.0	0.0	0.0	0.0	0.0	0.0	0.0	0.0	0.0	0.0	0.0	0.0	0.0	0.0	0.0	0.0	0.0	0.0	0.0	0.0	0.4
Fe	2.2	1.1	2.6	2.1	2.7	1.5	0.3	0.4	0.8	1.5	0.5	0.9	1.5	2.2	0.9	1.6	1.0	0.4	1.2	1.9	9.2	1.0	2.1	3.2	5.8
Sum	98.9	98.5	99.2	99.4	99.6	99.6	99.4	99.6	99.6	99.3	99.6	98.9	99.1	99.6	99.5	97.2	99.0	99.5	98.7	99.5	99.2	99.4	99.1	99.3	98.9
Structural formula (atoms per $(OH)_2$ O_{10})																									
Interlayer																									
Ca^{2+}	0.05	0.04	0.03	0.14	0.10	0.03	0.08	0.04	0.06	0.04	0.02	0.09	0.01	0.02	0.15	0.03	0.04	0.02	0.01	0.02	0.02	0.04	0.01	0.09	0.03
Mg^{2+}	0.10	0.03	0.10	0.02	0.06	0.08	0.06	0.08	0.09	0.07	0.08	0.03	0.10	0.04	0.04	0.02	0.03	0.14	0.12	0.07	0.03	0.04	0.11	0.13	0.09
Na^{+}	0.01	0.02	0.18	0.00	0.00	0.01	0.02	0.00	0.00	0.00	0.00	0.01	0.10	0.09	0.05	0.20	0.16	0.11	0.16	0.19	0.07	0.01	0.03	0.00	0.00
K^{+}	0.06	0.01	0.02	0.01	0.05	0.04	0.03	0.02	0.01	0.06	0.02	0.03	0.02	0.02	0.01	0.06	0.04	0.01	0.06	0.19	0.09[a]	0.02	0.23	0.12	0.03
Fe^{3+}	0.00	0.00	0.00	0.00	0.00	0.00	0.00	0.00	0.00	0.00	0.00	0.00	0.00	0.00	0.00	0.00	0.00	0.00	0.00	0.00	0.00	0.00	0.00	0.00	0.00
VI sheet																									
Cr^{3+}	0.00	0.00	0.00	0.00	0.00	0.00	0.00	0.00	0.00	0.00	0.00	0.00	0.00	0.00	0.00	0.00	0.00	0.00	0.00	0.00	0.00	0.00	0.00	0.00	0.03
Al^{3+}	1.30	1.63	1.29	1.37	1.36	1.51	1.60	1.67	1.50	1.36	1.69	1.59	1.52	1.46	1.45	1.43	1.60	1.49	1.44	1.49	0.24	1.59	1.54	1.06	0.65[b]
Fe^{3+}	0.45	0.20	0.46	0.29	0.49	0.28	0.06	0.07	0.16	0.30	0.09	0.17	0.25	0.36	0.16	0.32	0.17	0.06	0.21	0.32	1.74	0.21	0.31	0.55	1.19
Mg^{2+}	0.20	0.15	0.16	0.33	0.12	0.20	0.31	0.25	0.33	0.31	0.21	0.23	0.22	0.15	0.38	0.19	0.19	0.44	0.33	0.16	0.00	0.16	0.12	0.36	0.15
Ti^{4+}	0.01	0.01	0.01	0.01	0.02	0.01	0.01	0.01	0.02	0.03	0.01	0.01	0.01	0.02	0.01	0.02	0.01	0.01	0.01	0.01	0.01	0.04	0.02	0.02	0.02
IV sheet																									
Al^{3+}	0.08	0.01	0.13	0.01	0.24	0.07	0.00	0.01	0.00	0.01	0.01	0.05	0.08	0.09	0.06	0.07	0.06	0.02	0.13	0.34	0.39	0.05	0.40	0.23	0.15
Si^{4+}	3.92	3.99	3.87	3.99	3.76	3.93	4.00	3.99	4.00	3.99	3.99	3.95	3.92	3.91	3.94	3.93	3.94	3.98	3.87	3.66	3.61	3.95	3.60	3.77	3.85
XII	0.36	0.17	0.45	0.33	0.38	0.28	0.33	0.25	0.31	0.30	0.21	0.27	0.34	0.25	0.44	0.36	0.34	0.44	0.48	0.56	0.39	0.19	0.53	0.56	0.28
n^{VI}	1.97	2.00	1.92	2.00	1.99	1.99	1.99	2.00	2.00	2.00	2.00	2.00	1.99	1.99	2.00	1.96	1.97	2.01	1.99	1.98	2.00	1.99	1.96	1.99	1.93
%*S* (in %)	93 ±	107 ±	83 ±	107 ±	64 ±	95 ±	109 ±	107 ±	109 ±	107 ±	107 ±	99 ±	93 ±	91 ±	97 ±	95 ±	97 ±	105 ±	83 ±	49 ±	42 ±	99 ±	65 ±	66 ±	80 ±
± SDOM	2	4	1	3	3	3	3	1	1	1	1	2	2	3	2	4	1	1	3	2	2	2	3	3	3

Notes: VI sheet = octahedral sheet; IV sheet = tetrahedral sheet; XII = interlayer charges, n^{VI}: number of octahedral cation, %*S*: smectitic layer ratio; SDOM = standard deviation of mean; MX = MX80[2005]; Frd = Friedland clay; GH = GeoHellas clay; VN = Vietnam clay; [a] including 0.07 of interlayer Fe^{3+}, [b] including 0.08 of octahedral Cr^{3+}

Table 4. Chemical analyses of major elements by TEM-EDX (atom.%) and calculated mineral formula (cations per $[O_{10}(OH)_2]$) for mean of dioctahedral smectites from reaction products of (20 rpm + NaCl) and (60 rpm + NaCl) experiments.

Sample	04F 20r	04F 60r	09F 20r	09F 60r	11F 20r	11F 60r	12F 20r	12F 60r	16F 20r	16F 60r	#20 20r	#22a 20r	#23 20r	#23 60r	#24 60r	#27 20r	#27 60r	#30 20r	#32 20r	#32 60r	#31 20r	#33a 60r	MX 20r	MX 60r
Chemical analyses of major elements (atom.%) by TEM-EDX																								
Elements																								
O	62.8	62.5	62.2	62.7	63.1	66.5	61.5	63.2	63.6	62.2	62.1	62.8	62.9	67.9	67.2	64.1	68.2	63.1	62.3	61.9	61.7	81.6	62.6	62.9
Na	0.0	0.0	0.0	0.0	0.0	0.0	0.0	0.0	0.0	0.0	1.4	1.9	2.2	3.1	0.5	2.4	0.6	1.1	0.2	1.4	1.0	0.2	0.0	0.0
Mg	1.8	2.0	2.3	2.1	1.6	1.7	3.1	2.7	1.7	1.7	1.8	1.4	2.3	1.9	2.8	1.3	1.3	3.1	2.4	2.5	1.2	0.4	2.4	2.4
Al	9.0	8.3	9.2	9.9	8.3	7.8	7.8	7.8	9.0	9.2	9.5	8.5	8.3	6.6	7.2	8.9	8.3	8.1	10.0	9.2	11.0	2.5	9.5	9.2
Si	23.4	23.9	23.4	23.1	23.4	20.6	24.4	23.0	23.2	24.2	22.9	21.6	22.1	14.8	20.3	21.4	19.1	23.0	22.4	21.3	20.8	9.0	23.9	23.9
K	0.2	0.2	0.2	0.1	0.1	0.4	0.1	0.6	0.3	0.3	0.1	0.6	0.2	0.5	0.4	0.1	0.4	0.1	0.3	0.6	1.5	0.3	0.2	0.2
Ca	0.4	0.2	0.5	0.5	0.7	0.7	0.5	0.4	0.3	0.6	0.2	0.1	0.7	0.7	0.2	0.1	0.1	0.3	0.7	0.2	0.1	0.2	0.4	0.3
Ti	0.1	0.2	0.4	0.3	0.1	0.1	0.2	0.2	0.1	0.1	0.1	0.1	0.1	0.1	0.1	0.1	0.1	0.1	0.0	0.0	0.1	0.1	0.1	0.1
Fe	2.3	2.7	1.9	1.3	2.6	2.2	2.4	2.0	1.8	1.8	1.5	1.8	0.9	0.7	0.7	1.0	1.0	0.3	1.2	1.3	1.9	4.5	1.0	0.9
Sum	100.0	100.0	100.0	100.0	100.0	100.0	100.0	100.0	100.0	100.0	99.5	98.9	99.6	96.2	99.3	99.5	99.2	99.3	99.6	98.5	99.3	98.7	100.0	100.0
Structural formula (atoms per $(OH)_2$ O_{10})																								
Interlayer																								
Ca^{2+}	0.04	0.06	0.08	0.09	0.13	0.11	0.06	0.08	0.09	0.05	0.02	0.02	0.01	0.12	0.04	0.03	0.02	0.05	0.02	0.12	0.02	0.09	0.05	0.06
Mg^{2+}	0.10	0.09	0.10	0.09	0.05	0.05	0.09	0.12	0.04	0.06	0.07	0.05	0.09	0.02	0.11	0.08	0.05	0.10	0.13	0.09	0.07	0.12	0.09	0.09
Na^{+}	0.00	0.00	0.00	0.00	0.00	0.00	0.00	0.00	0.00	0.00	0.20	0.18	0.32	0.13	0.09	0.10	0.20	0.15	0.14	0.04	0.15	0.04	0.00	0.00
K+	0.03	0.04	0.02	0.03	0.07	0.02	0.10	0.01	0.05	0.06	0.01	0.11	0.13	0.03	0.09	0.08	0.02	0.02	0.11	0.06	0.26	0.09[a]	0.03	0.03
Fe^{3+}	0.00	0.00	0.00	0.00	0.00	0.00	0.00	0.00	0.00	0.00	0.00	0.00	0.00	0.00	0.00	0.00	0.00	0.00	0.00	0.00	0.00	0.02	0.00	0.00
VI sheet																								
Al^{3+}	1.29	1.38	1.50	1.36	1.29	1.31	1.25	1.22	1.44	1.47	1.48	1.42	1.40	1.44	1.40	1.56	1.57	1.46	1.43	1.48	1.50	0.16	1.52	1.51
Fe^{3+}	0.45	0.38	0.21	0.30	0.42	0.43	0.35	0.38	0.29	0.29	0.25	0.33	0.17	0.16	0.13	0.21	0.19	0.06	0.23	0.20	0.33	1.79	0.15	0.17
Mg^{2+}	0.23	0.22	0.24	0.28	0.28	0.23	0.37	0.39	0.25	0.21	0.23	0.22	0.41	0.39	0.45	0.19	0.18	0.48	0.33	0.31	0.14	0.03	0.31	0.30
Ti^{4+}	0.03	0.02	0.04	0.06	0.01	0.02	0.03	0.03	0.01	0.02	0.01	0.01	0.01	0.01	0.02	0.01	0.01	0.01	0.01	0.01	0.01	0.02	0.02	0.02
IV Sheet																								
Al^{3+}	0.10	0.12	0.16	0.16	0.17	0.09	0.03	0.03	0.06	0.07	0.12	0.13	0.24	0.06	0.05	0.13	0.06	0.03	0.21	0.21	0.40	0.56[b]	0.02	0.05
Si^{4+}	3.90	3.88	3.84	3.84	3.83	3.91	3.97	3.97	3.94	3.93	3.88	3.87	3.76	3.94	3.95	3.87	3.94	3.97	3.79	3.79	3.60	3.44	3.98	3.95
XII	0.30	0.33	0.37	0.39	0.43	0.33	0.41	0.39	0.31	0.29	0.41	0.40	0.65	0.45	0.49	0.40	0.35	0.48	0.55	0.52	0.59	0.57	0.31	0.33
n^{VI}	2.00	2.00	2.00	2.00	2.00	1.99	2.00	2.01	1.99	1.99	1.97	1.98	2.00	2.00	2.00	1.97	1.97	2.00	2.00	2.00	1.98	2.00	2.00	2.00
$\Delta\%S$	–4%	–8%	–29%	–29%	–7%	8%	–4%	–4%	2%	0%	–8%	–8%	–33%	0%	4%	–14%	0%	–2%	–14%	–14%	–8%	–20%	6%	0%

Notes: Calculation of the degree of alteration $\Delta\%S = \%S_{experiment} - \%S_{origin}$, ($\%S_{experiment}$ = % smectitic layers after experimental run, $\%S_{origin}$ = % smectitic layers of the initial material), based on TEM-EDX analyses; SDOM = standard deviation of mean; $\Delta\%S < 0$ = illitization; $\Delta\%S > 0$ = smectitization; XII = interlayer charges, n^{VI} = number of octahedral cations; 20r, 60r = 20 rpm or 60 rpm experiment; [a] including 0.02 of interlayer Fe^{3+}, [b] including 0.01 of tetrahedral Fe^{3+}

a larger Fe+Mg-ratio in the octahedral sheet compared with Belle Fourche, Pioche, and 11F bentonites. Δ%*S* values indicating changes in %*S* of the products in comparison with the original were also noted in samples of 04F, 09F, 12F, 16F, and MX80 (Table 4).

Moderate transport-controlled alteration experiments in contact with 1 M NaCl-solution (20 rpm + NaCl). Thirteen different bentonites were treated with 1 M NaCl solution, and treated by overhead rotating at 20 rpm for 30 days at room temperature (20 rpm + NaCl). The

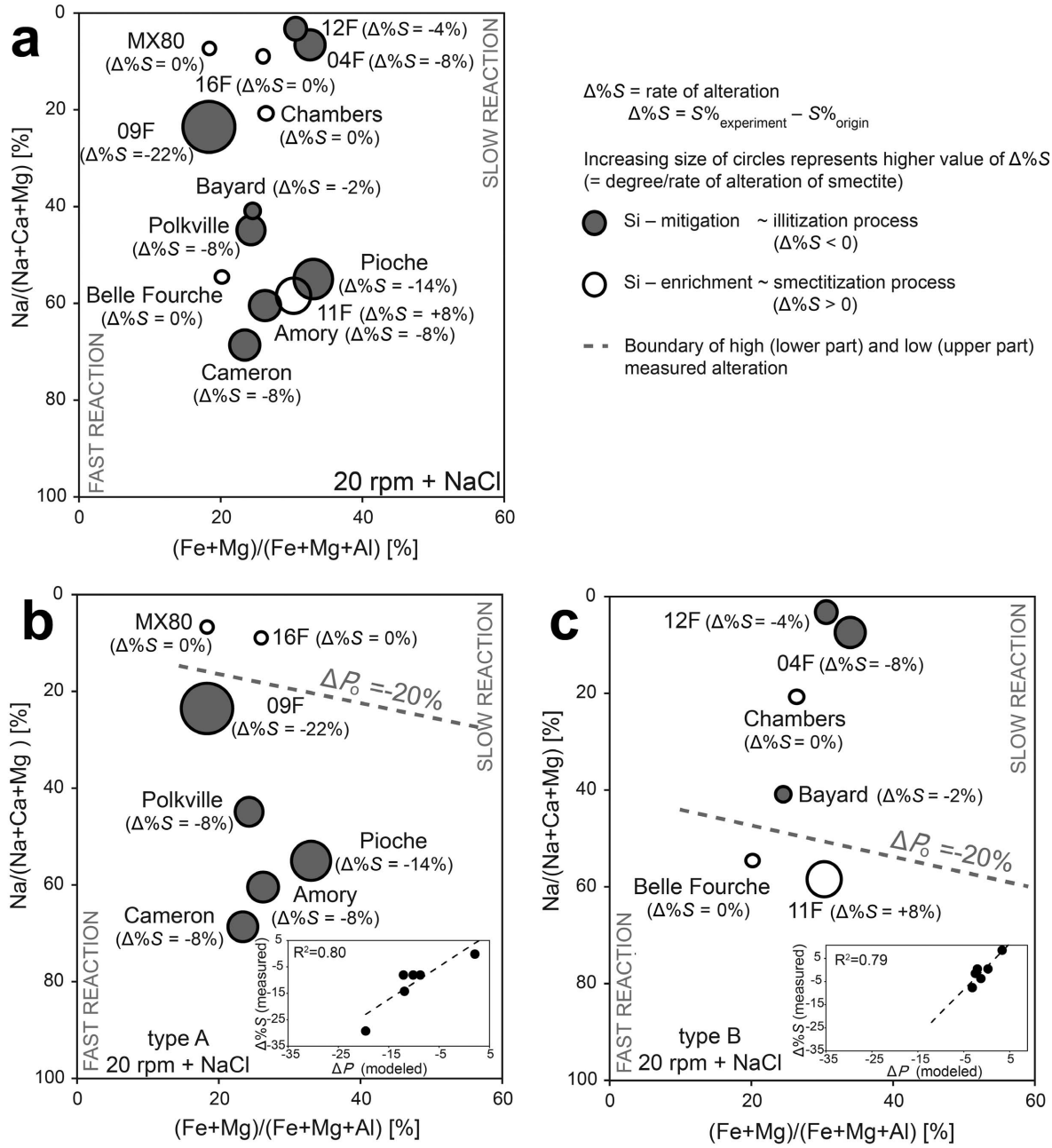

Figure 4. Smectitization and illitization caused by the (20 rpm + NaCl) experiment. (a) Results with all measured samples; (b) modeling of type A bentonites; and (c) modeling of type B bentonites using a flow rate of shaking of $\Delta P_o = -20\%$. Insets in parts b,c show verification between the modeled specific dissolution potential (ΔP) and the measured rate of alteration ($\Delta\%S$). Note: the horizontal and vertical axes represent the original compositions of the smectites. The diameters of the circles are related to measured loss or increase of the smectitic layer ratio, %*S*, between the original and the treated smectites (see note in Figure 2).

https://doi.org/10.1346/CCMN.2014.0620506 Published online by Cambridge University Press

parameter Δ%*S* (Table 4, Figure 4a), was similar to the (60 rpm + NaCl) experiment, and also indicated a reduced illitization due to the increase in Na content in the interlayer for the Cameron, Amory, Pioche bentonites and for the Polkville, and 09F bentonites (Figure 4b). The 09F bentonite has also shown indications of additional impact on the octahedral sheet. The other bentonites: 12F, 04F, Chambers, Bayard, Belle Fourche, and 11F, displayed different behavior (Figure 4c).

Highly transport-controlled alteration experiments in contact with deionized water (60 rpm + H_2O). Short-term experiments were carried out using eight samples saturated with deionized water and exposed to overhead rotating at 60 rpm for 30 days (60 rpm + H_2O). The calculated Δ%*S* values (Table 5) showed alteration processes in all of the samples and both smectitization and illitization were observed. No clear trend in the development of tetrahedral sheets in comparison to reduced or increased interlayer charge was found. At the end of the experiment the interlayer contained no Na.

Moderate transport-controlled alteration experiments in contact with deionized water (20 rpm + H_2O). The reaction products of overhead rotated bentonites and clays, investigated by TEM-EDX, indicated an alteration of between Δ%*S* ≈ −20% (illitization) for the 09F bentonite as well as the GeoHellas clay and Δ%*S* ≈ 30% (smectitization) for the Friedland clay (Table 5). The octahedral Fe+Mg-ratio showed a wide range, but the interlayer Na-ratio was limited. Illitization occured in the samples of GeoHellas, 09F, and 12F, while smectitization was observed in the samples of Vietnam, Friedland clay, 04F, and MX80.

Verification of mineral formulae calculated for original bentonites

The chemical data for each original bentonite and reaction product were determined by TEM-EDX (Tables 3–5). The mineral formulae calculated from TEM-EDX data were verified by FTIR measurements. A comparison of TEM-EDX-based octahedral Al *vs*. FTIR-based position of the δ_{AlAlOH}-band and octahedral Fe *vs*. δ_{AlFeOH}-band shows two different trends. These trends divide the samples into two groups referred to as types A and B (Figure 5). This comparison between TEM-EDX-based mineral formulae and FTIR measurements has shown strong linear trends within each group. The positions of the δ_{AlAlOH}-bands show an opposite linear trend for samples of type A or B in comparison to the development of octahedral Al measured by TEM-EDX (Figure 5a with significant coefficients of determination, R^2, for type A was 0.81 and for type B was 0.90). The positions of δ_{AlFeOH} bands moved to higher wavenumbers in the cases of decreasing octahedral Fe analyzed by TEM-EDX (Figure 5b with R^2 for type A was 0.75 and

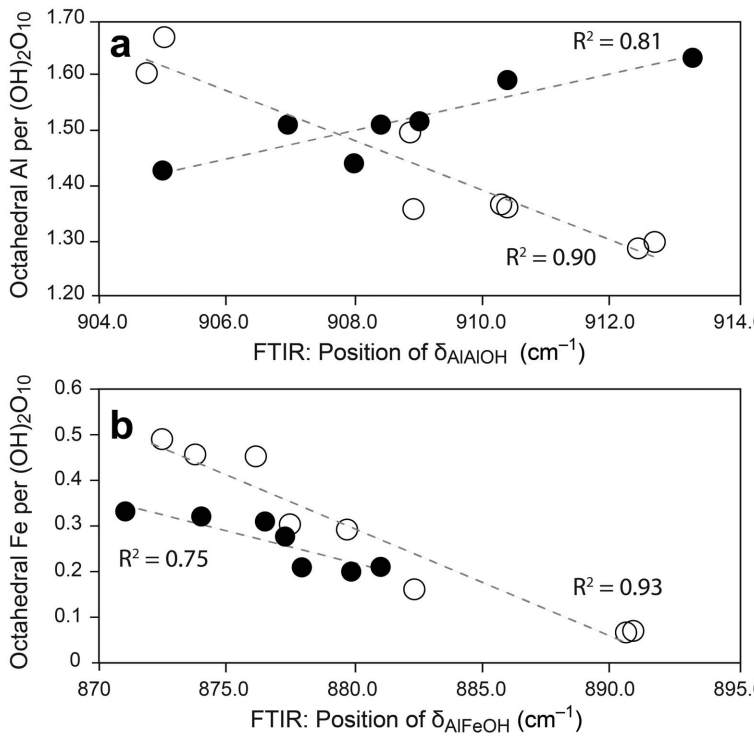

Figure 5. Chemical parameters classifying bentonites as members of type A (filled circles) or type B (open circles) with respect to their alteration in experimental series of (20 rpm +NaCl), (20 rpm + H_2O), and (60 rpm + H_2O): (a) verification of TEM-EDX-based octahedral Al-values by FTIR; and (b) verification of TEM-EDX-based octahedral Fe-values by FTIR.

https://doi.org/10.1346/CCMN.2014.0620506 Published online by Cambridge University Press

Table 5. Chemical analyses of major elements by TEM-EDX (atom.%) and calculated mineral formula (cations per $[O_{10}(OH)_2]$) for mean of dioctahedral smectites from reaction products of (20 rpm + H_2O) and (60 rpm + H_2O) experiments.

Sample	04F 20r	04F 60r	09F 20r	09F 60r	12F 20r	12F 60r	16F 20r	16F 60r	MX 20r	MX 60r	Frd 20r	Frd 60r	GH 20r	GH 60r	VN 20r	VN 60r	#22a 20r
Chemical analyses of major elements (atom.%) by TEM-EDX																	
Elements																	
O	63.8	62.8	61.9	63.1	62.7	63.8	64.9	63.9	65.6	63.4	75.9	65.0	62.5	63.2	67.4	62.2	62.8
Na	0.0	0.0	0.0	0.0	0.0	0.0	0.0	0.0	0.0	0.0	0.0	0.0	0.0	0.0	0.0	0.0	1.9
Mg	1.8	2.0	2.3	1.9	3.1	2.4	1.7	1.8	1.5	2.2	0.7	1.0	2.8	3.4	1.6	2.2	1.4
Al	8.9	9.1	9.6	9.4	7.8	7.7	8.8	9.0	9.4	9.4	6.8	10.1	8.7	6.0	3.6	3.5	8.5
Si	23.1	23.5	24.0	23.7	23.8	23.7	22.7	23.3	22.3	23.4	14.3	21.0	21.8	22.6	20.3	24.3	21.6
K	0.1	0.1	0.1	0.1	0.1	0.1	0.1	0.2	0.1	0.1	0.6	1.0	1.0	0.5	0.2	0.1	0.6
Ca	0.1	0.1	0.3	0.3	0.5	0.1	0.1	0.1	0.2	0.3	0.1	0.0	0.1	0.2	0.1	0.2	0.1
Ti	0.1	0.2	0.2	0.2	0.1	0.1	0.1	0.1	0.1	0.2	0.1	0.1	0.1	0.1	0.1	0.1	0.1
Fe	2.1	2.2	1.5	1.4	1.8	2.2	1.6	1.5	0.9	1.0	1.0	1.6	3.1	4.0	6.1	7.2	1.8
Sum	100	100	100	100	100	100	100	100	100	100	99.5	99.8	100	100	99.4	99.7	98.9
Structural formula (atoms per $(OH)_2$ O_{10})																	
Interlayer																	
Ca^{2+}	0.02	0.02	0.04	0.05	0.02	0.08	0.02	0.02	0.05	0.03	0.01	0.02	0.04	0.02	0.03	0.02	0.02
Mg^{2+}	0.12	0.10	0.07	0.11	0.12	0.11	0.10	0.08	0.09	0.07	0.09	0.07	0.16	0.16	0.12	0.11	0.12
Na^{+}	0.00	0.00	0.00	0.00	0.00	0.00	0.00	0.00	0.00	0.00	0.00	0.00	0.00	0.00	0.00	0.00	0.00
K+	0.03	0.02	0.02	0.02	0.01	0.01	0.03	0.02	0.02	0.02	0.18	0.16	0.10	0.20	0.01	0.05	0.03
Fe^{3+}	0.00	0.00	0.00	0.00	0.00	0.00	0.00	0.00	0.00	0.00	0.00	0.00	0.00	0.00	0.00	0.00	0.00
VI sheet																	
Al^{3+}	1.40	1.41	1.53	1.46	1.32	1.27	1.51	1.48	1.54	1.63	1.58	1.55	0.94	1.26	0.51[a]	0.57[b]	1.40
Fe^{3+}	0.36	0.37	0.26	0.24	0.37	0.31	0.26	0.31	0.16	0.16	0.28	0.30	0.70	0.46	1.18	1.20	0.36
Mg^{2+}	0.21	0.21	0.18	0.26	0.29	0.41	0.21	0.21	0.27	0.19	0.10	0.12	0.33	0.29	0.24	0.19	0.21
Ti^{4+}	0.03	0.01	0.02	0.04	0.02	0.02	0.01	0.01	0.03	0.02	0.01	0.02	0.03	0.01	0.02	0.01	0.03
IV sheet																	
Al^{3+}	0.13	0.07	0.06	0.12	0.02	0.04	0.04	0.02	0.06	0.04	0.22	0.21	0.17	0.35	0.09	0.11	0.13
Si^{4+}	3.87	3.93	3.94	3.88	3.98	3.96	3.96	3.98	3.94	3.96	3.78	3.79	3.83	3.65	3.91	3.89	3.87
XII	0.31	0.26	0.26	0.35	0.29	0.40	0.26	0.22	0.30	0.22	0.39	0.35	0.49	0.55	0.31	0.31	0.31
n^{VI}	2.00	2.00	1.99	2.00	2.00	2.01	1.99	2.00	2.00	2.00	1.98	1.99	2.00	2.03	1.95	1.97	2.00
$\Delta\%S$	−10%	2%	−10%	−22%	−2%	−6%	6%	10%	−2%	2%	27%	29%	10%	−19%	11%	7%	−10%

Notes: Calculation of degree of alteration $\Delta\%S = \%S_{experiment} - \%S_{origin}$, ($\%S_{experiment}$ = % smectitic layer after experimental run, $\%S_{origin}$ = % smectitic layer of the initial material), based on TEM-EDX analyses; SDOM = standard deviation of mean; $\Delta\%S < 0$ = illitization; $\Delta\%S > 0$ = smectitization; XII = interlayer charges, n^{VI} = number of octahedral cations; 20r, 60r = 20 rpm or 60 rpm experiment; [a] and [b] including 0.05 of octahedral Cr^{3+}.

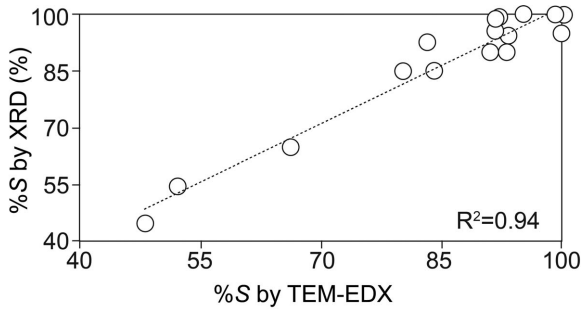

Figure 6. Comparison of smectitic layer ratio, %*S*, of original material determined by TEM with results of XRD (ethylene-glycol saturation of oriented mounts, of the <2 μm fraction) according to Moore and Reynolds (1997).

for type B was 0.93). The %*S* values determined by TEM-EDX measurements were also verified by XRD of ethylene glycol-saturated oriented mounts (Figure 6). The approach of Moore and Reynolds (1997) to determine illitic layer ratio by locating second- and third-order interferences of the smectitic phase (Figure 7) gave a significant linear trend between $\%S_{TEM}$ and $\%S_{XRD}$ with a coefficient of determination of 0.94 (Figure 6).

DISCUSSION

Influence of interlayer and octahedral cations, and flow rate of fluid movement, on the rate of alteration and stability of bentonite

The results obtained indicate that each sample tested in the experiments showed a different development of the tetrahedral sheet. The full spectrum from illitization to a slight smectitization was identified. Alteration of Si content in tetrahedral sheets in all the samples was demonstrated by Δ%*S* values (Tables 4, 5). Moreover, the tetrahedral sheets seemed to be changed abruptly from stronger illitization into slight smectitization. This development is seen in the (60 rpm + NaCl) experiments (Figure 3), where a change from decreasing Na-ratio released the high illitization of the Chambers sample (Δ%*S* = −33%) and switched it to a slight smectitization as seen in samples such as 16F (Δ%*S* = +2%) and MX80 (Δ%*S* = +6%). This Na-ratio defines the group of samples, classified as type A.

During the course of the alteration experiments, any dissolution or precipitation process could be affected by migration of dissolved Si from the tetrahedral sheet and of other cations, mainly from the interlayer. The dissolved Si and the cations could be released by a transport-controlled process into the aqueous solution by the overhead rotation. The effect of such mitigation is defined here as the degree of alteration by flow rate of fluid movement from rotating activity which is expressed as Δ*P*o. The Δ*P*o coefficient is derived from the observed sudden change of the Δ%*S* values from strong illitization to slight smectitization (Figure 3). The present study assumed that the dissolution of Si was greater for some samples than the rate of removal of dissolved Si by fluid movement. In cases of greater Si dissolution, the unmitigated dissolved Si should be precipitated and result in newly formed montmorillonite layers (*i.e.* the beginning of smectitization). For each of the experiments, the Δ*P*o value was determined empirically, based on the measured Δ%*S* values. The same procedure was applied to determine the impact of the initial composition of octahedral cations using the Fe+Mg-ratio. From their modeled Δ*P* values, the bentonites studied are grouped into three categories of high, medium, or low rate of alteration (Table 6) and

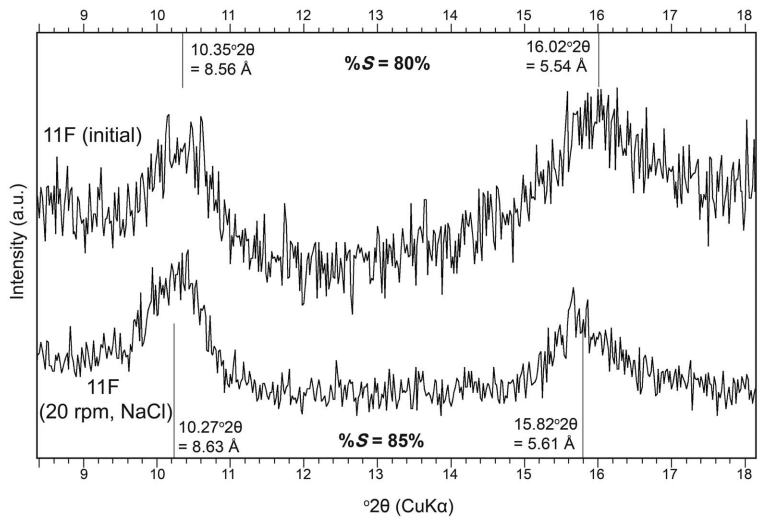

Figure 7. Determination of smectitic layer ratio, %S, by XRD (ethylene-glycol saturation of oriented mounts, <2 μm fraction) in accordance with Moore and Reynolds (1997): sample 11F (original material and after experiments with 20 rpm + NaCl).

https://doi.org/10.1346/CCMN.2014.0620506 Published online by Cambridge University Press

Table 6. Specific dissolution potential (ΔP) of bentonite classified by short-term alteration experiments.

Bentonite in contact with 1 M NaCl solution at highly transport-controlled alteration experiments (60 rpm + NaCl)						Bentonite in contact with deionized water at highly and little transport-controlled alteration experiments (60 rpm + H_2O, 20 rpm + H_2O)				
Samples		Type	ΔP_{XII} (%)	ΔP_{VI} (%)	ΔP (%)			Type	ΔP_{XII} (%)	ΔP_{VI} (%)	ΔP (%)
	28F	A	−103	−6	−109 ± 1		Garfield	B	−18	−76	−94 ± 4
	37F	A	−103	−4	−107 ± 1	FR-B	11F	B	−18	−8	−26 ± 1
	31F	A	−87	−7	−94 ± 1		MX80	A	−20	−5	−24 ± 2
	GeoHellas	A	−76	−10	−86 ± 2		16F	A	−16	−6	−22 ± 2
	23F	A	−71	−5	−76 ± 2		Vietnam	B	0	−15	−15 ± 2
	Vietnam	A	−60	−11	−71 ± 3		09F	A	−11	−4	−15 ± 5
	13F	A	−55	−7	−63 ± 3		Bayard	B	−16	4	−12 ± 1
FR-B	12F	A	−55	−7	−62 ± 3		Polkville	A	−6	−6	−11 ± 1
	38F	A	−42	−6	−48 ± 5	MR-B	Pioche	A	−5	−6	−11 ± 2
	04F	A	−39	−7	−46 ± 5		Amory	A	−5	−6	−11 ± 2
	MX80	A	−40	−5	−46 ± 5		GeoHellas	B	0	−9	−9 ± 1
	16F	A	−33	−6	−39 ± 5		Cameron	A	−4	−6	−9 ± 2
	22F	A	−31	−5	−36 ± 6		Otay	A	−2	−6	−8 ± 1
	Chambers	A	−23	−7	−30 ± 6		Chambers	B	−9	4	−6 ± 2
	9F	A	−21	−5	−26 ±11		12F	B	0	−1	−1 ± 1
	Garfield	A	−7	−12	−19 ± 5		13F	B	0	−1	−1 ± 1
	Bayard	A	−10	−7	−17 ± 3		31F	B	0	−1	−1 ± 1
	Polkville	A	−10	−6	−16 ± 1		04F	B	−1	0	0 ± 4
	Amory	A	−8	−7	−15 ± 5		38F	B	0	6	0 ± 1
MR-B	Pioche	A	−7	−7	−14 ± 4	SR-B	23F	B	0	10	0 ± 2
	11F	A	−6	−8	−14 ± 1		28F	B	0	3	0 ± 1
	Cameron	A	−6	−6	−12 ± 6		37F	B	0	11	0 ± 1
	Belle Fourche	A	−6	−5	−12 ± 2		Belle Fourche	B	−19	30	0 ± 2
	Otay	A	−2	−7	−9 ± 2		22F	B	−5	30	0 ± 2

Notes: ΔP_{XII} = impact of interlayer cations on the stability of smectite; ΔP_{VI} = impact of octahedral cations on the stability of smectite; $\Delta P = \Delta P_{XII} + \Delta P_{VI}$ = specific dissolution potential of smectite; SR-B = Slow-reacting bentonite, MR-B = Moderate-reacting bentonite, FR-B = Fast-reacting bentonite.

referred to as SR-B ($\Delta P < -5\%$), MR-B ($-5\% < \Delta P < -20\%$), or FR-B ($\Delta P > -20\%$), respectively.

Highly transport-controlled alteration experiments in contact with 1 M NaCl solution (60 rpm + NaCl). The measured values of $\Delta\%S$ and the Na-ratios from the samples of Otay, 11F, Pioche, Chamber, and 16F with similar Fe+Mg-ratios (Table 4, Figure 3) were applied to correlate the impact of interlayer (ΔP_{XII}) on the specific dissolution potential (ΔP) resulting in the progression equation (Figure 2a, equation 3):

$$\Delta P_{XII} = 15.09 \ln [Na/(Na+Ca+Mg)] - 68.26 \quad (3)$$

The measured values of $\Delta\%S$ and the Fe+Mg-ratios from the samples of Belle Fourche, 11F, Pioche, and Garfield, which have similar Na-ratios, were correlated describing the impact of the octahedral sheet (ΔP_{VI}) on the specific dissolution potential (ΔP) by using the regression equation (Figure 2b, equation 4):

$$\Delta P_{VI} = -4.36 \ln [(Fe+Mg)/(Fe+Mg+Al)] - 7.47 \quad (4)$$

Based on the measured $\Delta\%S$ values (Table 4) as well as the modeled ΔP_{XII} and ΔP_{VI} values (Table 6), the ΔPo parameter was computed empirically to be −35% for the (60 rpm + NaCl) experiments (above the Chambers bentonite) (Figure 3). This value means that the rotating activity at 60 rpm in 1 M NaCl solution results in a flow rate removing dissolved Si corresponding to a potential for illitization of smectite of −35%. A larger available amount of dissolved Si coupled with a smaller flow rate causes smectitization as a result. Calculated ΔP (Table 6) indicated that most of the clays and bentonites in this experiment act as FR-B and MR-B.

Based on a comparison of the two factors, ΔP_{XII} and ΔP_{VI}, on the dissolution potential, this research has shown systematic trends between the Na-ratios (Figures 2a, 8a) in the interlayer and the Fe+Mg-ratio (Figures 2b, 8b) in the octahedral sheets *vs.* ΔP. A good correlation between the ΔP values and the measured $\Delta\%S$ values of all reaction products of the (60 rpm + NaCl) experiment ($R^2 = 0.90$ for $n = 11$) verified that the hypothesis has a robust basis related to a coupled cation layer substitution and charge balance. The $\Delta\%S$ values of the analyzed samples revealed that large quantities of interlayer Na and octahedral Al generate a stable smectite structure as found in the Otay bentonite. This Na-rich smectite is relatively resistant to alteration and is therefore classified as a slow-reacting bentonite.

https://doi.org/10.1346/CCMN.2014.0620506 Published online by Cambridge University Press

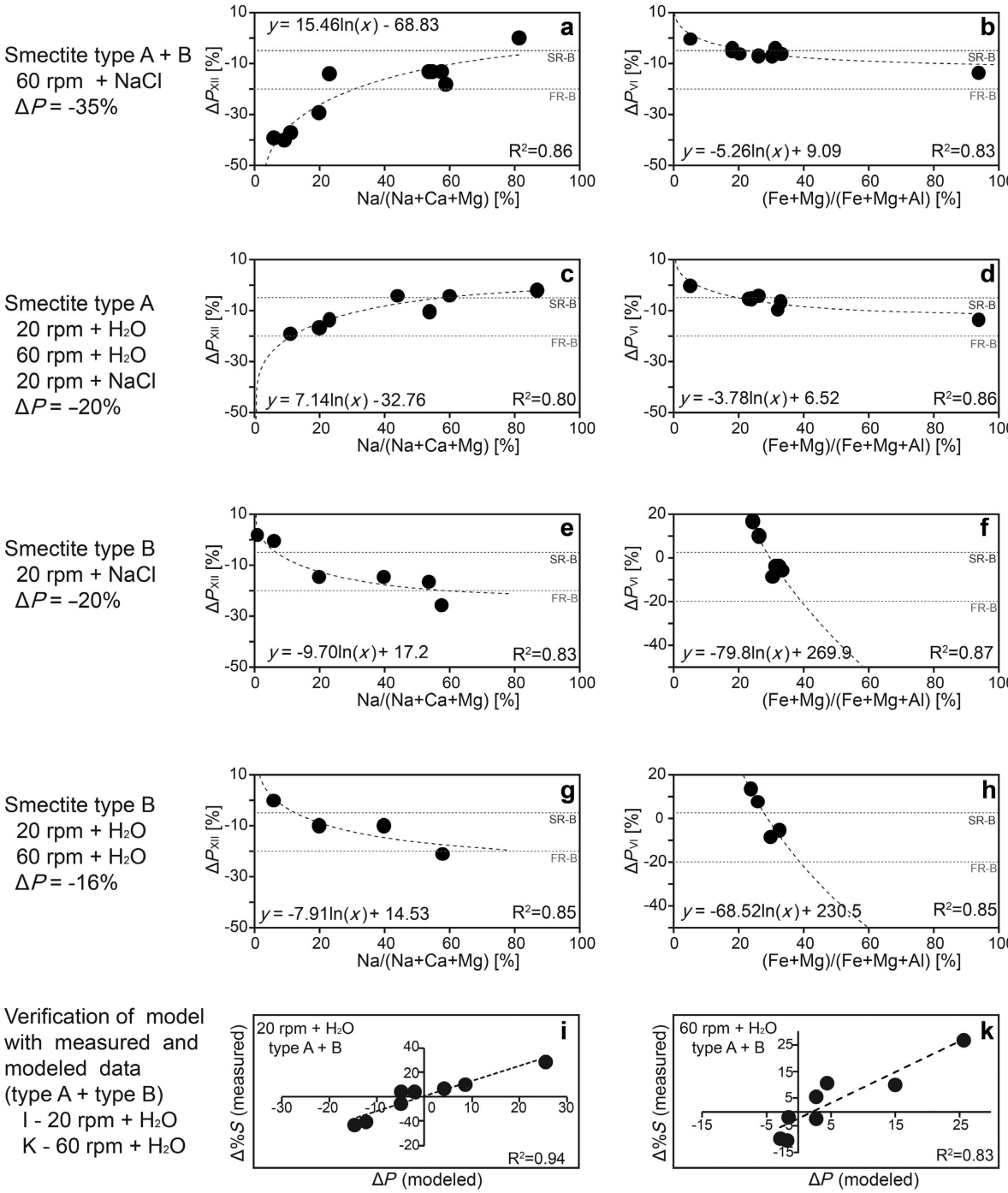

Figure 8. Modeling the different impact of interlayer cations (ΔP_{XII}) and octahedral cations (ΔP_{VI}) on specific dissolution potential (ΔP) for the different experimental designs. $\Delta P = \Delta P_{XII} + \Delta P_{VI}$.

Larger amounts of Ca+Mg in the interlayer and/or octahedral Fe and Mg cations increase the dissolution rate of smectite by promoting the release of Si. Illitization occurs as long as the value of dissolved Si is smaller than the extent of Si mitigation caused by the overhead rotating activity (flow rate of fluid movement from overhead rotation $-\Delta P$o) under the applied experimental conditions. Smectitization follows if the amount of dissolved Si is greater than the Si mitigation potential resulting from the ΔPo value. Intense dissolution can also override the potential of smectitization, if a %*S* of close to 100% was achieved. Clogging caused by

https://doi.org/10.1346/CCMN.2014.0620506 Published online by Cambridge University Press

the resulting non-mitigated Si would be expected to lead to local precipitation and cementation of Si material (*e.g.* dark area in Figure 3).

Moderate transport-controlled alteration experiments in contact with 1 M NaCl solution (20 rpm + NaCl). For all of the samples studied, no significant correlation could be found between the measured Δ%*S* either with the Na-ratios or with the Fe+Mg-ratios (Figure 4a). The alteration process involved here is therefore different from that seen in the (60 rpm + NaCl) experiments. Due to the differences in their transformation behavior, the bentonites were divided into two types, A and B. Bentonites of type A included Cameron, Amory, Pioche, Polkville, MX80, 09F, and 16F (Figure 4b). Based on the measured Δ%*S* values for these samples (Table 4) and the models of ΔP_{XII} and ΔP_{VI} (Figures 8c,d), a suitable Δ*P*o value was computed to be −20% (Figure 4b). Bentonites of type B include 04F, 11F, 12F, Chambers, Bayard, and Belle Fourche (Figure 4c). Here, a larger interlayer Na-ratio (in contrast to type A) and a large octahedral Fe+Mg-ratio of the dominant smectite phase in type B enhanced the rate of alteration, in the direction of illitization. Thus, a large initial Ca+Mg ratio in the interlayer and a small octahedral Fe+Mg-ratio protected the particles against dissolution processes (Figures 8e,f). The Δ*P*o of −20% for the bentonites of type A, and the same assumed flow rate in the (20 rpm + NaCl) experiment, is thus also suitable for the bentonites of type B (Figure 4c) with their ΔP_{XII} and ΔP_{VI} models (Figures 8e,f). Strong correlations were found between measured Δ%*S* and modeled Δ*P* for both types and these are presented in the small boxes in Figure 4b,c.

Highly transport-controlled alteration experiments in contact with deionized water (60 rpm + H_2O). As with the (20 rpm + NaCl) experiment, the alteration behavior of the bentonites with the (60 rpm + H_2O) experiment showed a weak trend between illitization and smectitization (Table 5). The alteration behavior will therefore be discussed by using the same classification into types A and B bentonite as was used for the (20 rpm + NaCl) experiment. The modeled ΔP_{XII} and ΔP_{VI} values (Table 6) indicated a trend for greater illitization related to lower interlayer Na-ratios. A greater octahedral Fe+Mg-ratio was identified for the 09F, 16F, MX80, and Friedland, which are bentonites of type A. Thus, increasing interlayer Na-ratios and decreasing octahedral Fe+Mg-ratios protect smectite particles against dissolution processes (Figures 8c,d). The other samples have shown behavior related to Ca+Mg ratios of type B. The Vietnam and GeoHellas clays were characterized by a high dissolution potential. The amount of their dissolved Si was greater than could be removed by the estimated flow rate. The reaction products of these samples have, consequently, exhibited smectitization (Figures 8g,h). The Δ*P*o of this experiment was computed as −16%. For all of the samples, both types A and B, comparison between the modeled Δ*P* and the measured Δ*S* indicates strong correlation with R^2 = 0.83 for this (60 rpm + H_2O) experiment (Figure 8i).

Moderate transport-controlled alteration experiments in contact with deionized water (20 rpm + H_2O). Similar to the (20 rpm + NaCl) and (60 rpm + H_2O) experiments, the bentonites and clays can be divided into two types. Bentonites of type A include 09F, 16F, MX80, and Friedland; bentonites of type B include 04F, 12F, Geohellas, and Vietnam. The Δ*P*o value derived from the ΔP_{XII} and ΔP_{VI} values for bentonites of type A (Figures 8c,d) and the ΔP_{XII} and ΔP_{VI} values for bentonites of type B (Figures 8g,h) are −16%. For all of type A and type B bentonites, the modeled Δ*P* correlated strongly with the measured Δ%*S* (R^2 = 0.94 for this experiment) (Figure 8k).

Classification of bentonite as type A and type B

From the discussion above, different interlayer composition-related mechanisms could explain the occurrence of two classes of bentonite, types A and B (Table 6). In bentonites of type A, Na^+ cations in interlayer of the dominant smectite phases acted as stabilizers. In type B, in contrast, bentonites and clays were stabilized by relatively large amounts of interlayer Ca^{2+} and Mg^{2+} cations. The presence of the Ca^{2+} cation as a protecting mechanism (type B) occurred only in experimental designs of 20 rpm + NaCl, 60 rpm + H_2O, and 20 rpm + H_2O, and it indicates the occurrence of two different types of behavior. In both types, a larger Fe+Mg-ratio in the octahedral sheets generally caused a greater rate of alteration. The initial composition of the octahedral sheet discriminates these two bentonite types (Figure 9). The original bentonites of type A were characterized by octahedral $Al^{3+}_{VI} > 1.4$ and $Fe^{3+}_{VI} > 0.2$ per $[O_{10}(OH)_2]$. The original octahedral composition of the second group of samples followed the limits (1) $Al^{3+}_{VI} <$ 1.4 per $[O_{10}(OH)_2]$ and $Fe^{3+}_{VI} > 0.2$ per $[O_{10}(OH)_2]$ or (2) $Al^{3+}_{VI} > 1.4$ per $[O_{10}(OH)_2]$, and $Fe^{3+}_{VI} < 0.2$ per $[O_{10}(OH)_2]$ (Figure 9).

Muller *et al.* (2000) and Wolters (2005) used thermal analysis to classify smectites into three types. Based on their octahedral Al^{3+} and Fe^{3+} contents, those authors identified smectites with $Al^{3+}_{VI} < 1.4$ per $[O_{10}(OH)_2]$ and $Fe^{3+}_{VI} > 0.3$ per $[O_{10}(OH)_2]$ which were *trans*-vacant; the smectites with $Al^{3+}_{VI} > 1.4$ per $[O_{10}(OH)_2]$ and $Fe^{3+}_{VI} < 0.3$ per $[O_{10}(OH)_2]$ were *cis*-vacant, and the smectites with $Al^{3+}_{VI} > 1.4$ per $[O_{10}(OH)_2]$ and $Fe^{3+}_{VI} > 0.3$ per $[O_{10}(OH)_2]$ tended to be *trans*-vacant mostly and were predominantly ferrian. Following the findings of Muller *et al.* (2000) and Wolters (2005), type B contained *trans*-vacant (for $Al^{3+}_{VI}<1.4$ per $[O_{10}(OH)_2]$ and $Fe^{3+}_{VI}>0.3$ per $[O_{10}(OH)_2]$) and *cis*-vacant bentonites (for $Al^{3+}_{VI}>1.4$ per $[O_{10}(OH)_2]$ and $Fe^{3+}_{VI}<0.3$ per $[O_{10}(OH)_2]$) as well as which type A is occupied by *trans*-vacant members (for $Al^{3+}_{VI} >1.4$ per $[O_{10}(OH)_2]$ and $Fe^{3+}_{VI} >0.3$ per $[O_{10}(OH)_2]$). The relation between *cis* and *trans*

https://doi.org/10.1346/CCMN.2014.0620506 Published online by Cambridge University Press

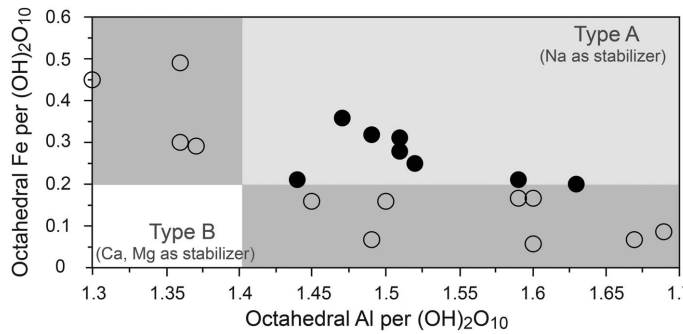

Figure 9. Differentiation of bentonites into types A or B controlled by the distribution of octahedral Al and Fe. Filled circles = bentonite of type A with Na acting as the stabilizing interlayer cation; open circles = bentonite of type B with Ca+Mg acting as stabilizing cations.

vacancies of clay minerals alone is, therefore, insufficient to explain the alteration potential of clays/bentonites.

The classification of clays/bentonites into types A or B was best achieved in the present study by FTIR analyses, which permit the analysis of the composition of octahedral sheets of smectite (as shown in Figure 5). Smectites of type A show δ_{AlAlOH} bands with increasing wavenumbers resulting from increasing octahedral Al content, while smectites of type B are characterized by an inverse relationship of decreasing wavenumbers of δ_{AlAlOH} bands related to large octahedral Al contents (Figure 5a). This may be driven by initial cation content controlling the potential substitution in octahedral and tetrahedral sheets of the initial smectite (Gates, 2005). Two negative correlations, for type A and type B, can be found between amounts of octahedral Fe and wavenumbers of δ_{AlFeOH} bands (Figure 5b). Comparing smectites from types A and B bentonites yields the same wavenumber of δ_{AlFeOH}-bands, smectites of type B contain larger amounts of Fe than do smectites of type A. The large quantities of Fe are probably facilitated by primary environmental conditions giving the cation availability for an earlier (early diagenetic) occupation of Fe^{3+} into the *trans*-octahedral positions of natural smectites in type A, as opposed to that in type B.

Geological origin of bentonite as further impact for specific dissolution potential

The environmental conditions in which the clays and bentonites are formed lead to different structural chemical compositions of smectites which predict the specific alteration potential of smectite. These thus serve as a geological fingerprint. According to Seim and Tischendorf (1990), the amount of Al and Fe in the octahedral sheet was the result of the pH environment during smectite formation in the deposits. The dominant smectite phases in bentonites/clays of type A were associated with a neutral pH-milieu (pH = 5.0–7.0), where Al^{3+} and Fe^{3+} were found preferentially. Bentonites of type B were formed in an alkaline pH environment (from pH 7.5 to 9.0), where Fe^{2+} was stabilized in the structure of smectite. In such environments, Fe^{2+} in the lattice position can later be reduced *in situ* by oxidation and Al^{3+} remains in large concentrations in the octahedral sheet. Sampling locations in deposits and the parent rocks are also contributory factors. Grim and Güven (1978), Christidis and Makri (2007), and Christidis (2008) showed that the chemical compositions of the dominant smectite in clays and bentonites could vary significantly from center to margin or bottom to top in any of the deposits. Garrels and Christ (1965) and Christidis (2008) investigated the relationship between parent rocks and the amount of Fe in the octahedral sheet and found that smectites from basic rocks were characterized by mean Fe^{3+} contents of 0.63 per $[O_{10}(OH)_2]$, from intermediate rocks, by 0.21 Fe^{3+} per $[O_{10}(OH)_2]$, and from acidic rocks by 0.12 Fe^{3+} per $[O_{10}(OH)_2]$; Fe^{3+} was mobile only at very low pH and very high Eh environmental conditions. Tetrahedral Si also mirrored parent rocks but not as clearly as octahedral Fe. Smectites from basic rocks showed a trend with 3.73 Si^{4+} per $[O_{10}(OH)_2]$, from intermediate rock with 3.82 Si^{4+} per $[O_{10}(OH)_2]$, and from acidic rocks with 3.92 Si^{4+} per $[O_{10}(OH)_2]$. In conclusion, the parent rock type and the original depositional environment during bentonite formation affect the structural and chemical composition of smectites in clays or bentonites. This chemical composition also determines the specific alteration potential, ΔP.

The classification of all bentonites and clays investigated by their specific dissolution potential (ΔP) in the overhead rotating treatment experiments and the impact of the smectitic layer (%*S*) are summarized in Table 6. From this analysis, the Bayard, Pioche, Cameron, Amory, Polkville, Otay, and Belle Fourche bentonites are suitable bentonites for use as buffer and backfill materials in the HLW repository.

Mechanism of alteration and relevance for HLW repositories

The composition of the octahedral sheet showed that larger Fe+Mg-ratios increased the alteration rate of smectites. The larger ion diameter of Fe and Mg in

https://doi.org/10.1346/CCMN.2014.0620506 Published online by Cambridge University Press

comparison to Al caused greater structural stresses which reduced the resistance of particles. This explanation is in agreement with the views of Čičel and Novak (1977), and Novak and Čičel (1978), who studied the alteration of smectites in acid environments. The composition of the interlayer also strongly affects the degree of alteration of smectite. Kaufhold and Dohrmann (2008) suggested that Ca-montmorillonite is more stable than Na-montmorillonite. Na^+ will be more easily detached than Ca^{2+} from the interlayer into colloidal particles at low ionic strength. Laird (2006) claimed that an increase in the amount of Na^+ (type A) in the interlayer can enhance the viscosity of water in the interlayer or can enlarge the co-volume swelling between the particles. Both mechanisms result in the limitation of particle movement, and thus Na-smectites have greater resistance. A large Na concentration therefore has the effect of retarding the dissolution impact on smectite particles and favors delamination of relatively stable quasicrystals. For Na-dominant populations of the interlayer, a co-volume process increases the swelling pressure between the delaminated layers as the particle number increases (Laird, 2006). As a result the co-volume processes cause a limitation of the particle mobility during rotating activities. Such Na-montmorillonites have only a low specific dissolution potential and are considered to be stable phases. According to the proposed categorization, they belong to slow-reacting bentonite.

In the other cases, type B bentonite with charges oriented opposite to one another on adjacent layers will be protected. Divalent cations (Ca, Mg) in the interlayer can fix the sheet stacks and balance the opposing charges in adjacent layers. The smectite will be protected from alteration by an increase in the overall stack stability. Due to the relative number of platelets per tactoid and hydrolysis properties, Ca-montmorillonite is more stable than Na-montmorillonite in water (Banin and Lahav, 1968; Eyal and Singer, 1987; Kaufhold and Dohrmann, 2008). An increase in the number of Ca+Mg cations in the interlayer promotes the unmixing of monovalent and divalent cations to particles of different sheet structures. Quasicrystals can therefore be broken along Na-bearing interlayer and help to maintain the quasicrystal (Laird, 2006). Such bentonite with Ca- and Mg-montmorillonites can be also taken as slow-reacting bentonite due to their low specific dissolution potential.

Speeds of overhead rotating were interpreted as affecting flow rates of fluid movement in the experiments described here. The effect of the flow rate of fluid movement on the Si content of smectite causing a smectitization or illitization has been described by Pusch and Kasbohm (2002), Herbert *et al.* (2004), and Kasbohm *et al*. (2013). The flow rate of groundwater along the interface between the granite host rock and barriers in a repository can transport the detached colloidal particles from compacted bentonites (Pusch, 1999a). The hydraulic regime in the system is also important for the reaction path. Si mitigation (illitization) happens in an open system, when the rate of Si dissolution is lower than the flow rate induced by rotating. Si enrichment (smectitization) will occur if the Si dissolution is greater than the flow rate induced by rotating. Smectitization is therefore to be expected in closed systems, although it is not excluded in open systems, especially in cases of a high specific dissolution potential. The rapid smectitization of smectite is characterized by amounts of tetrahedral Si close to 4.0 per $[O_{10}(OH)_2]$. At higher values, Si aggregated preferentially and precipitated from the solution. Si clogging in the microstructures of smectite (interstitial porosity) can then affect the barrier performance (Pusch, 1999b; Xiaodong *et al.*, 2011; Kasbohm *et al*., 2013). Kasbohm *et al.* (2002) and Herbert *et al.* (2011) also found indications that the Si buffer of the MX-80 bentonite can transform dissolved Si into the lattice structure of illite-smectite interstratified structures. This leads to a transformation of former illite layers into montmorillonite layers by recrystallization of Si. Si cementation consequently can have a more drastic impact on the properties of engineered barriers than the illitization processes and is therefore relevant for the geometry of HLW repositories.

CONCLUSIONS

Using the 25 bentonites dominated by smectite and/or illite-smectite interstratified phases, this research has demonstrated that each bentonite has a specific dissolution potential reflecting its stability during short-term alteration. The main factor influencing the stability of smectite is the interlayer and octahedral compositions. Those bentonites classified as type A (with $Al^{3+}_{VI} > 1.4$ and $Fe^{3+}_{VI} > 0.2$ per $[O_{10}(OH)_2]$) are more stable because of "co-volume swelling" where Na^+ is the dominant ion in the interlayers of the smectite. By contrast, type B bentonites (with $Al^{3+}_{VI} > 1.4$ and $Fe^{3+}_{VI} < 0.2$ or $Al^{3+}_{VI} < 1.4$ and $Fe^{3+}_{VI} > 0.2$ per $[O_{10}(OH)_2]$) are more stable in cases with low Na concentrations in the interlayer because of the significant unmixing of the monovalent and divalent (Ca^{2+} and/or Mg^{2+}) interlayer cations. Larger quantities of Fe and/or Mg in the octahedral sheets of the two types of bentonite enhanced their rates of alteration because of the associated stress in the interlayers which affects the particle lattice structure. This finding is in agreement with previous studies concerning the stability of smectites (Čičel and Novak, 1977). The composition of the octahedral sheet is determined largely by the pH condition during the formation of the bentonite (a geochemical fingerprint).

The impact of fluid movement (*e.g.* percolation flow rate) and the ratio of smectitic layers within the illite-smectite interstratifications are shown to be factors of smectitization and illitization processes. Bentonite, with

https://doi.org/10.1346/CCMN.2014.0620506 Published online by Cambridge University Press

illite-smectite interstratifications, is a preferred candidate material for an engineered barrier because of its large buffer potential for the incorporation of aqueous Si and the formation of a new, expandable smectitic layer. Alternatively, smectitization of fully developed montmorillonite (Si_{IV} ~ 4.0 [$O_{10}(OH)_2$]) can lead to Si cementation that can have more drastic impacts on engineered barrier materials than the process of illitization. In the present study, the Belle Fourche bentonite was characterized as a suitable candidate for a HLW barrier from a chemical-mineralogical perspective. Using a range of techniques to determine the chemical composition of bentonite, such as TEM-EDX and FTIR measurements, it is possible to estimate its dissolution potential and select a suitable material for engineered barriers.

ACKNOWLEDGMENTS

The current study was supported by Gesellschaft für Anlagen- und Reaktorsicherheit (GRS) GmbH under contract No 02 E 10538 with the Federal Ministry of Economics and Technology (BMWi), Germany. The authors acknowledge gratefully the support of the Mineralogical Laboratories of the Ernst-Moritz-Arndt-Universität Greifswald, Germany. They also thank Prof. Bob Jack and Dr Barry Rawlins for improving the manuscript. The Associate Editor and the Editor in Chief are thanked for their valuable comments and suggestions, which helped the authors to improve the final version of this manuscript.

REFERENCES

Adamcova, J., Hanusova, I., Ponavic, M., and Prikryl, R. (2008) Alteration processes in bentonites. P. 19 in*: Book of Abstracts of 18th Clay Conference in the Czech Republic* (Stastny, M., editor).

Banin, A. and Lahav, N. (1968) Particle size and optical properties of montmorillonite in suspension. *Israel Journal of Chemistry*, **6**, 235–250.

Bauer, A., Schäfer, T., Dohrmann, R., Hoffmann, H., and Kim, J.I. (2001) Smectite stability in acid salt solutions and the fate of Eu, Th and U in solution. *Clay Minerals*, **36**, 93–103.

Bergmann, J., Friedel, P., and Kleeberg, R. (1998) BGMN – a new fundamental parameter based Rietveld program for laboratory X-ray sources, its use in quantitative analysis and structure investigations. *CPD Newsletter*, **20**, 5–8.

BGR (2007) Nuclear waste disposal in Germany: Investigation and evaluation of regions with potentially suitable host rock formations for a geologic nuclear repository. *Report of the Bundesanstalt für Geowissenschaften und Rohstoffe*, Hannover/Berlin, 17 pp.

Bildstein, O., Trotignona, L., Perronnet, M., and Jullien, M. (2006) Modelling iron–clay interactions in deep geological disposal conditions. Parts A/B/C. *Physics and Chemistry of the Earth*, **31**, 10–14.

Carlson, L., Karnland, O., Oversby, M., Rance, A.P., Smart, N.R., Snellman, M., Vähänen, M., and Werme, O. (2007) Experimental studies on the interaction between anaerobically corroding iron and bentonite. *Physics and Chemistry of the Earth*, **32**, 334–335.

Castellanos, E., Villar, M.V., Romero, E., Lloret, A., and Gens, A. (2008) Chemical impact on the hydro-mechanical behaviour of high-density FEBEX bentonite. *Physics and Chemistry of the Earth*, **33**, 5516–5526.

Charpentier, D., Devineau, K., Mosser-Ruck, R., Chathelineau, M., and Villieras, F. (2006) Bentonite–iron interactions under alkaline condition: An experimental approach. *Applied Clay Science*, **32**, 1–13.

Christidis, G.E. (2008) Do bentonites have contradictory characteristics? An attempt to answer unanswered questions. *Clay Minerals*, **43**, 515–529.

Christidis, G.E. and Makri, P. (2007) Distribution of layer charge and charge distribution of smectites in bentonite deposits: Implications for bentonite genesis. *Abstracts volume, Euroclay2007, Aveiro, Portugal*.

Christidis, G.E., Katsiki, P., Pratikakis, A., and Kacandes, G. (2010) Rheological properties of palygorskite-smectite suspensions from the Ventzia Basin, W. Macedonia, Greece. Pp. 2562–2569 in: *Bulletin of the Geological Society of Greece*. Proceedings of the 12th International Congress.

Čičel, B. and Novak, I. (1977) Dissolution of smectites in hydrochloric acid. I. Half-time of dissolution as a measure of reaction rate. Pp. 163–171 in: *Proceedings of the 7th Conference on Clay Mineralogy and Petrology* (J. Konta, editor). Charles University, Prague, Czechoslovakia.

Craciun, C. (1984) Influence of the Fe^{3+} for Al^{3+} octahedral substitutions on the IR spectra of montmorillonite minerals. *Spectroscopy Letters*, **17**, 579–590.

Dixon, D.A., Gray, M.N., and Graham, J. (1996) Swelling and hydraulic properties of bentonites from Japan, Canada and USA. Proceedings of the 2nd International Congress on Environmental Geotechnics, Osaka, Japan, pp. 5–8.

Eyal, B.D. and Singer, A. (1987) Optical density of vertisol clay suspensions in relation to sediment volumes and dithionite-citrate-bicarbonate-extractable iron. *Clays and Clay Minerals*, **35**, 311–317.

Farmer, V.C. (1974) *The Infrared Spectra of Minerals*. Mineralogical Society, London, 539 pp.

Farmer, V.C. and Russell, J.D. (1964) The infrared spectra of layer silicates. *Spectrochimica Acta*, **20**, 1149–1173.

Ferrage, E., Lanson, B., Sakharov, B.A., and Drits, V.A. (2005) Investigation of smectite hydration properties by modeling experimental X-ray diffraction patterns: Part I. montmorillonite hydration properties. *American Mineralogist*, **90**, 1358–1374.

Garrels, R.M. and Christ, C.L. (1965) *Solutions, Minerals, and Equilibria*. Harper, London, 464 pp.

Gates, W.P. (2005) Infrared spectroscopy and the chemistry of dioctahedral smectites. Pp.126–168 in: *Vibrational Spectroscopy of Layer Silicates and Hydroxides* (T. Kloprogge, editor). CMS Workshop Lecture Series, **14**, The Clay Minerals Society, Aurora, Colorado, USA.

Goodman, B.A., Russell, J.D., Fraser, A.R., and Woodhams, F.W.D. (1976) A Mössbauer and IR spectroscopic study of the structure of nontronite. *Clays and Clay Minerals*, **24**, 52–59.

Grim, R.E. and Güven, N. (1978) *Bentonites – Geology, Mineralogy, Properties and Uses*. Developments in Sedimentology, **46**. Elsevier, New York, 254 pp.

Herbert, H.J., Kasbohm, J., and Henning, K.H. (2004) Long-term behaviour of the Wyoming bentonite MX-80 in high saline solutions. *Applied Clay Science*, **26**, 275–291.

Herbert, H.-J., Kasbohm, J., Sprenger, H., Fernández, A.M., and Reichelt, C. (2008) Swelling pressures of MX-80 bentonite in solutions of different ionic strength. *Physics and Chemistry of the Earth*, **33**, 327–342.

Herbert, H.-J., Kasbohm, J., Nguyen, T.L., Meyer, L., Hoang, T.M.T., and Xie, M. (2011) Fe-bentonite – Experiments and modeling of the interactions of bentonites with iron. In: *Gessellschaft für Anlange und Reaktiosicherheit* – report, No. **295**, Braunschweig, Germany, ISBN 978-3-939355-72-4, 302 pp.

Hoang-Minh, T. (2006) Characterization of Clays and Clay

Minerals for Industrial Applications: Substitution of Non-natural Additives by Clays in UV Protection. PhD thesis, Ernst-Moritz-Arndt-University Greifswald, Germany, 184 pp.

Honty, M., Uhlík, P., Šucha, V., Čaplovičová, M., Franců, J., Clauer, N., and Biroň, A. (2004) Smectite-to-illite alteration in salt-bearing bentonites (the East Slovak basin). *Clays and Clay Minerals*, **52**, 533–551.

Ishidera, T., Ueno, K., Kurosawa, S., and Suyama, T. (2008) Investigation of montmorillonite alteration and formation of iron corrosion products in compacted bentonite in contact with carbon steel for 10 years. *Physics and Chemistry of the Earth*, **33**, 269–275.

Karnland, O., Olsson, S., and Nilsson, U. (2006) Mineralogy and sealing properties of various bentonites and smectite-rich clay materials. In: *Technical Report of SKB TR-06-30*, SKB, Stockhlom, Sweden, 112 pp.

Karnland, O., Olsson, S., Nilsson, U., and Sellin, P. (2007) Experimentally determined swelling pressures and geochemical interactions of compacted Wyoming bentonite with highly alkaline solutions. *Physics and Chemistry of the Earth*, **32**, 275–286.

Kasbohm, J., Tarrah, J., and Henning, K.-H. (2002) Transmissionselektronen-mikroskopische Untersuchungen an Feinfraktionen der Ringversuchsprobe "Ton Stoob". Pp. 71–84 in: *Beiträge zur Jahrestagung Wien, 18.-20.9. 2002. Berichte der Deutschen Ton- und Tonmineralgruppe e.V. Band 9* (F. Ottner and S. Gier, editors).

Kasbohm, J., Pusch, R., and Henning, K.-H. (2004) Short term experiments with different bentonites in saline solutions. In: *Berichte der DTTG, Karslruhe 10* (R. Nüesch and K. Emmerich, editors).

Kasbohm, J., Pusch, R., Nguyen-Thanh, L., and Hoang-Minh, T. (2013) Lab-scale performance of selected expandable clays under HLW repository conditions. *Environmental Earth Science*, **69**, 2569–2579.

Kaufhold, S. and Dohrmann, R. (2008) Detachment of colloidal particles from bentonites in water. *Applied Clay Science*, **39**, 50–59.

Kaufhold, S. and Dohrmann, R. (2009) Stability of bentonites in salt solutions: I. sodium chloride. *Applied Clay Science*, **45**, 171–177.

Kaufhold, S. and Dohrmann, R. (2010) Stability of bentonites in salt solutions: II. Potassium chloride solution – Initial step of illitization? *Applied Clay Science*, **49**, 98–107.

Kaufhold, S. and Dohrmann, R. (2011) Stability of bentonites in salt solutions: III. Calcium hydroxide. *Applied Clay Science*, **51**, 300–307.

Kaufhold, S. and Dohrmann, R. (2013) The variable charge of dioctahedral clay minerals. *Journal of Colloid and Interface Science*, **390**, 225–233.

Kaufhold, S., Dohrmann, R., Koch, D., and Houben, G. (2008) The pH of aqueous bentonite suspensions. *Clays and Clay Minerals*, **56**, 338–343.

Kaufhold, S., Dohrmann, R., and Klinkenberg, M. (2010) Water uptake capacity of bentonites. *Clays and Clay Minerals*, **58**, 37–43.

Kleeberg, R., Ufer, K., and Bergmann, J. (2010) Rietveld analysis with BGMN–Rietveld method physical basics profile modelling quantification. In: *BGMN workshop Freiberg 2010*. Technische Universität Bergakademie Freiberg. Freiberg, Germany, 87 pp.

Köster, H.M. (1977) Die Berechnung kristallchemischer Strukturformeln von 2:1-Schichtsilikaten unter Berücksichtigung der gemessenen Zwischenschichtladungen und Kationenaustauschkapazitäten, sowie die Darstellung der Ladungsverteilung in der Struktur mittels Dreieckskoordinaten. *Clay Minerals*, **12**, 45–54.

Laird, D.A. (2006) Influence of layer charge on swelling of smectites. *Applied Clay Science*, **34**, 74–87.

Madejová, J. and Komadel, P. (2001) Baseline studies of the Clay Minerals Society Source Clays: infrared methods. *Clays and Clay Minerals*, **49**, 410–432.

Madejová, J., Komadel, P., and Čičel, B. (1994) Infrared study of octahedral site populations in smectites. *Clay Minerals*, **29**, 319–326.

Madsen, F.T. (1998) Clay mineralogical investigations related to nuclear waste disposal. *Clay Minerals*, **33**, 109–129.

Marty, N.C.M., Fritz, B., Clement, A., and Michau, N. (2010) Modelling the long term alteration of the engineered bentonite barrier in an underground radioactive waste repository. *Applied Clay Science*, **47**, 82–90.

Meunier, A. and Velde, B. (2004) *Illite: Origin, Evolution and Metamorphism*. Springer, New York.

Mosser-Ruck, R., Cathelineau, M., Guillaume, D., Charpentier, D., Rousset, D., Barres, O., and Michau, N. (2010) Effects of temperature, pH, and iron/clay and liquid/clay ratios on experimental conversion of dioctahedral smectite to berthierine, chlorite, vermiculite, or saponite. *Clays and Clay Minerals*, **58**, 280–291.

Moore, D.M. and Reynolds, R.C. (1997) *X-ray Diffraction and the Identification and Analysis of Clay Minerals*, 2nd edition. Oxford University Press, New York, 332 pp.

Muller, F., Drits, V., Plançon, A., and Robert, J.-L. (2000) Structural transformation of 2:1 dioctahedral layer silicates during dehydroxylation-rehydroxylation reactions. *Clays and Clay Minerals*, **48**, 572–585.

Nguyen-Thanh, L. (2012) Mineralogical Characterization of Fe-driven Alteration in Smectites. PhD thesis, Ernst-Moritz-Arndt-University Greifswald, Germany, 213 pp.

Nguyen-Thanh, L., Hoang-Minh, T., Kasbohm, J., Herbert, J.-H., Nguyen, T.D., and Le, T.L. (2014) Characterization of Fe-smectites and their alteration potential in relation to engineered barriers for HLW repositories: The Nui Nua clay, Thanh Hoa province, Vietnam. *Applied Clay Science*, **101**, 168-176.

Novak, I. and Čičel, B. (1978) Dissolution of smectites in hydrochloric acid: II. Dissolution rate as a function of crystallochemical composition. *Clays and Clay Minerals*, **26**, 341–344.

Pearson, F.J., Arcos, D., Bath, A., Boisson, J.Y., Fernández, A.M., Gäbler, H.E., Gaucher, E., Gautschi, A., Griffault, L., Hernán, P., and Waber, H.N. (2003) Mont Terri Project – geochemistry of water in the Opalinus clay formation at the Mont Terri rock laboratory. Reports of the Federal Office for Water and Geology (FOWG). *Geology Series* **5**, 319 pp.

Perronnet, M., Jullien, M., Villiéras, F., Raynal, J., Bonnin, D., and Bruno, G. (2008) Evidence of a critical content in Fe(0) on FoCa7 bentonite reactivity at 80ºC. *Applied Clay Science*, **38**, 187–202.

Pusch, R. (1992) Use of bentonite for isolation of radioactive waste products. *Clay Minerals*, **27**, 353–361.

Pusch, R. (1999a) Microstructural evolution of buffers. *Engineering Geology*, **54**, 32–42.

Pusch, R. (1999b) Clay colloid formation and release from MX-80 buffer. *Technical Report Swedish Nuclear Fuel and Waste Management Co*, No. TR-99-31, Geodevelopment AB, Stockholm, Sweden, 36 pp.

Pusch, R. (2002) The Buffer and Backfill Handbook. Part 2: Materials and techniques. In: *Technical Report Swedish Nuclear Fuel and Waste Management Co*, No. TR 02-12, Stockholm, Sweden, 198 pp.

Pusch, R. and Kasbohm, J. (2002) Alteration of MX-80 by hydrothermal treatment under high salt content conditions. In: *Technical Report Swedish Nuclear Fuel and Waste Management Co*, No. TR 02-06, Stockholm, Sweden, 39 pp.

Pusch, R. and Yong R.N. (2006) *Microstructure of Smectite Clays and Engineering Performance*. Taylor and Francis, London

Seim, R. and Tischendorf, G. (1990) *Grundlagen der Geochemie*. VEB Deutscher Verlag für Grundstoffindustrie, Leipzig, Germany.

SKI (2005) Engineered barrier system – Long-term stability of buffer and backfill. In: *Swedish Nuclear Power Inspectorate report 2005*, No. 48, Stockholm, Sweden, 120 pp.

Środoń, J., Elsass, F., McHardy, W.J., and Morgan, D.J. (1992) Chemistry of illite-smectite inferred from TEM measurements of fundamental particles. *Clay Minerals*, **27**, 137–158.

Stober, I. and Bucher, K. (2002) Origin of salinity of deep groundwater in crystalline rocks. *Terra Nova*, **11**, 181–185.

Suzuki, S., Sazarashi, M., Akimoto, T., Haginuma, M., and Suzuki, K. (2008) A study of the mineralogical alteration of bentonites in saline water. *Applied Clay Science*, **41**, 190–198.

Ufer, K., Roth, G., Kleeberg, R., Stanjek, H., Dohrmann, R., and Bergmann, J. (2004) Description of X-ray powder pattern of turbostratically disordered layer structures with a Rietveld compatible approach. *Zeitschrift für Kristallographie*, **219**, 519–527.

Ufer, K., Stanjek, H., Roth, G., Dohrmann, R., Kleeberg, R., and Kaufhold, S. (2008) Quantitative phase analysis of bentonites by the Rietveld method. *Clays and Clay Minerals*, **56**, 272–282.

Wolters, F. (2005) Classification of montmorillonites. Dissertation, Universität Karlsruhe, Germany, 98 pp.

Xiaodong, L., Prikryl, R., and Pusch, R. (2011) THMC-testing of three expandable clays of potential use in HLW repositories. *Applied Clay Science*, **52**, 419–427.

(*Received 6 January 2014; revised 28 November 2014; Ms. 833; AE: A. Thompson*)